RIS-Assisted Receive Generalized Space Shift Keying and Receive Generalized Spatial Modulation

A Thesis submitted
to the College of Graduate and Postdoctoral Studies
In Partial Fulfillment of the Requirements
For the Degree of Master of Science
In the Department of Electrical and Computer Engineering
University of Saskatchewan
Saskatoon

By
Porfirio Ameth Marín Flores

Permission to Use

In presenting this thesis/dissertation in partial fulfillment of the requirements for a Post-graduate degree from the University of Saskatchewan, I agree that the Libraries of this University may make it freely available for inspection. I further agree that permission for copying of this thesis/dissertation in any manner, in whole or in part, for scholarly purposes may be granted by the professor or professors who supervised my thesis/dissertation work or, in their absence, by the Head of the Department of Electrical and Computer Engineering or the Dean of the College of Graduate Studies in which my thesis work was done. It is understood that any copying or publication or use of this thesis/dissertation or parts thereof for financial gain shall not be allowed without my written permission. It is also understood that due recognition shall be given to me and to the University of Saskatchewan in any scholarly use which may be made of any material in my thesis/dissertation.

Requests for permission to copy or to make other uses of materials in this thesis/dissertation in whole or in part should be addressed to:

Head of the Department of Electrical and Computer Engineering
57 Campus Drive
University of Saskatchewan
Saskatoon, Saskatchewan, Canada
S7N 5A9

OR

Dean of College of Graduate and Postdoctoral Studies
116 Thorvaldson Building, 110 Science Place
University of Saskatchewan
Saskatoon, Saskatchewan, Canada
S7N 5C9

Abstract

The introduction of the 5th-generation (5G) wireless communication standards has brought new applications and services that demand improved technologies to support growing traffic. To meet these demands, researchers have been exploring advanced 5G and future-oriented 6th-generation (6G) technologies. These envisioned technologies indicate the necessity for innovative communication paradigm shifts, especially at the physical layer. Consequently, there has been a growing interest in controlling the propagation channel, leading to the popularity of reconfigurable intelligent surfaces (RIS) as a potential approach for future wireless communications.

Recently, RIS has garnered attention as a potential solution to improve spectrum utilization and energy efficiency (EE). A typical standard RIS model consists of a two-dimensional metasurface of metallic or dielectric materials, equipped with a large array of subwavelength resonators. Software-defined manipulation of these elements modifies electromagnetic (EM) properties, enhancing the reflection of incident radio frequency (RF) signals. Another paradigm that is gaining interest in advancing communication systems is index modulation (IM). With IM schemes, the transmission of information bits occurs by activating or deactivating transmission/reception entities such as transmit antennas, receive antennas, and/or subcarriers. This introduces new dimensions for efficient information conveyance, potentially enhancing the spectral efficiency (SE). Hence, in this thesis, we focus on the combination of RIS-assisted systems with IM to further enhance the performance of future wireless communication systems.

In the first main contribution of the thesis, we enhance the performance of wireless communication systems by utilizing RIS and IM. In particular, we introduce two schemes: RIS-assisted receive generalized space shift keying (RIS-RGSSK) and RIS-assisted receive generalized spatial modulation (RIS-RGSM). In the RIS-RGSSK scheme, information bits are conveyed through selection of multiple receive antennas. The RIS-RGSM scheme takes RIS-RGSSK a step further by conveying information bits not only through the selection of multiple receive antennas but also through embedding information bits in the phase of the

received signals using M-ary phase shift keying (PSK) modulation. We also present simple yet efficient greedy detectors (GDs) for non-coherent detection of both schemes. Simulation results demonstrate the advantages of our proposed methods over existing schemes such as the RIS-assisted receive quadrature space-shift keying (RIS-RQSSK).

In the second main contribution of this thesis, we analyze the performance of the RIS-RGSSK and the RIS-RGSM. Specifically, we find closed-form expressions of the pairwise error probabilities (PEPs) of the RIS-RGSSK and the RIS-RGSM schemes when two antennas are activated at the receiver. Finally, we present comparisons of our analytical results with simulated-based results.

Acknowledgments

I am truly grateful for the support and encouragement I have received throughout my M.Sc. degree. This dissertation would not have been possible without the guidance and assistance of many individuals and organizations.

First and foremost, I would like to express my sincere gratitude to my supervisor, Dr. Ebrahim Bedeer Mohamed, and my co-supervisor Dr. Muhammad Hanif for their invaluable guidance, insightful feedback, and active support throughout my research. I am also thankful to my committee members for their constructive comments and suggestions.

I would like to extend my appreciation to the Department of Electrical and Computer Engineering at the University of Saskatchewan for providing an academic environment with the necessary resources for my research. In addition, I am grateful to the professors in this department for their knowledge-sharing during the courses I took here.

This degree was generously supported via a scholarship by the National Secretariat of Science, Technology, and Innovation of the Republic of Panama (SENACYT). Their financial assistance through the Graduate Scholarships Subprogram made this work possible.

I am very grateful to my family for their unconditional love and encouragement. To my parents, Maria and Porfirio, my two sisters, Kathia and Keyla, my nephew Alcibiades, my nieces Kamileth and Keily, and my grandparents Sofia and Modesto, your belief in me kept me going through the hardest challenges. A special thanks to my brother-in-law, Alcibiades, for his support.

To my friends, both near and far, thank you for your companionship, understanding, and the different ways you have supported me.

I would also like to acknowledge the Canadian community for their warm welcome during my time in Canada. Your kindness and hospitality have made my stay here a memorable experience.

Finally, I would like to thank anyone else who contributed to my research and personal

growth during this journey. Your support, whether big or small, has been greatly appreciated.

Thank you all.

Table of Contents

List of Figures

List of Abbreviations

5G	Fifth Generation (Cellular Network)
6G	Sixth Generation (Cellular Network)
AP	Access Point
APM	Amplitude-Phase Modulation
BER	Bit Error Rate
BS	Base Station
CD-IM	Channel-Domain Index Modulation
CF-mMIMO	Cell-Free Massive Multiple Input Multiple Output
CR	Cognitive Radio
CSI	Channel State Information
DCS	Digitally Controllable Scatterers
DH	Dual-Hop
DM-SCIM	Dual-Mode Single Carrier Index Modulation
DMBM	Differential Media-Based Modulation
EE	Energy Efficiency
EM	Electromagnetic
ESIM-OFDM	Enhanced Subcarrier Index Modulation with Orthogonal Frequency-Division Multiplexing
ESM	Enhanced Spatial Modulation
FD-IM	Frequency-Domain Index Modulation
FTN-IM	Faster-than-Nyquist Rate Index Modulation
GD	Greedy Detector
GSSK	Generalized Space Shift Keying
GSM	Generalized Spatial Modulation
IM	Index Modulation
IoT	Internet of Things
JRM	Joint Mapped Reflection Modulation
KKT	Karush-Kuhn-Tucker

LIS	Large Intelligent Surfaces
MBM	Media-Based Modulation
mMIMO	Massive Multiple Input Multiple Output
MIMO	Multiple Input Multiple Output
ML	Maximum Likelihood
mmWave	Millimeter Wave
MISO	Multiple Input Single Output
NOMA	Non-Orthogonal Multiple Access
OFDM	Orthogonal Frequency-Division Multiplexing
PSK	Phase Shift Keying
PEP	Pairwise Error Probability
QAM	Quadrature Amplitude Modulation
QPSK	Quadrature Phase Shift Keying
QRM	Quadrature Reflection Modulation
RF	Radio Frequency
RIS	Reconfigurable Intelligent Surface
RIS-ESM	RIS-Assisted Enhanced Spatial Modulation
RIS-JGD-GQRM	RIS-Assisted Joint Grouping Design Generalized QRM
RIS-RGSSK	RIS-Assisted Receive GSSK
RIS-RGSM	RIS-Assisted Receive GSM
RIS-RQSM	RIS-Assisted Receive Quadrature Spatial Modulation
RIS-RSSK	RIS-Assisted Receive Space Shift Keying
RIS-RSM	RIS-Assisted Receive Spatial Modulation
RPM	Reflection Pattern Modulation
RV	Random Variable
SC-IM	Single Carrier IM
SD-IM	Spatial-Domain IM
SE	Spectral Efficiency
SIM-OFDM	Subcarrier Index Modulation with OFDM
SIMO	Single Input Multiple Output

SM	Spatial Modulation
SNR	Signal-to-Noise Ratio
SCS	Software Controllable Surfaces
SSK	Space Shift Keying
TD-IM	Time-Domain IM
TI	Time Index
TIM	Time IM
UAV	Unmanned Aerial Vehicle
URLLC	Ultra-Reliable and Low Latency Communications

List of Publications

P. A. Marín, M. Hanif, and E. Bedeer, "RIS-assisted receive generalized space shift keying and receive generalized spatial modulation," *IEEE Wireless Commun. Lett.*, vol. 13, no. 10, pp. 2712–2716, Aug. 2024.

P. A. Marín, M. Hanif, and E. Bedeer, "Performance analysis of RIS-assisted receive generalized space shift keying and generalized spatial modulation," under review.

1. Introduction

1.1 Motivation

The 5th generation (5G) wireless communication standards have significantly transformed the industry by enabling more users and services, which in turn has led to a substantial increase in traffic demands. It is expected that this exponential growth might pose challenges in terms of spectrum efficiency, energy consumption, and overall network performance in future wireless communication systems. To meet the growing traffic demands, researchers have explored advanced 5G and future-oriented 6th-generation (6G) technologies [1]. These envisioned technologies highlight the necessity for innovative communication paradigm shifts, especially at the physical layer. Consequently, there has been a growing interest in technologies to control the propagation channel, leading to the popularity of reconfigurable intelligent surface (RIS) as a potential approach for future wireless communications [2], [3].

Recently, RISs have emerged as a promising solution to address these challenges. An RIS typically involves the use of surfaces composed of a large number of passive reflective elements that can control the phase shift and amplitude gain of incident electromagnetic (EM) waves. This capability allows the RIS to dynamically shape and control the propagation environment, thereby enhancing signal strength, reducing interference, and improving coverage in wireless networks. By intelligently directing signals, RIS can create favourable propagation conditions that can significantly boost the spectral efficiency (SE) and energy efficiency (EE) of wireless systems [4].

In parallel, index modulation (IM) has gained attraction due to its ability to increase the bits per channel usage by embedding additional information within the indices of ac-

tive transmission entities, such as antennas or subcarriers. IM schemes, including spatial modulation (SM) and space shift keying (SSK) can exploit the spatial dimension to convey extra information, thereby enhancing the SE. The combination of RIS and IM presents a compelling synergy: RIS can optimize the propagation channel to maximize the benefits of IM, while IM can leverage the controlled environment created by RIS to achieve higher data rates [5]. Hence, the combination of RIS and IM can potentially improve the SE in future wireless systems, particularly through innovative schemes such as RIS-assisted receive generalized space-shift keying (RIS-RGSSK) and RIS-assisted receive generalized spatial modulation (RIS-RGSM), which are central to the exploration in this thesis.

1.2 Research Objectives

There are two main objectives in this research:

- **Design the reflection coefficients of RIS to optimize the performance of both the RIS-RGSSK and RIS-RGSM to enhance the SE.** To achieve this objective, we formulate an optimization problem which maximizes the minimum value of the real part of the received signals at all the selected antennas. We firstly solve this optimization problem for the RIS-RGSSK scheme, and then we extend the RIS-RGSSK optimization solution to the RIS-RGSM scheme. Additionally, we present non-coherent greedy detectors (GDs) for both schemes.
- **Analyze the performance of the RIS-RGSSK and RIS-RGSM schemes, with optimized reflection coefficient, in terms of pairwise error probability (PEP).** To analyze the performance of both the RIS-RGSSK and RIS-RGSM schemes, we utilize the GD of each scheme. In order to achieve this objective with tractable derivations, we consider that two antennas are activated at the receiver.

1.3 Organization of the Thesis

This thesis is organized in a manuscript-based style.

This thesis has a total of five chapters. Chapter 1 introduces the motivation and research

objectives. Chapter 2 provides a comprehensive background on RIS and IM, detailing their basic principles, roles in future wireless systems, and applications. It also includes an extensive survey of related works on RIS, particularly focused on methods to increase data rates. The remaining part of the thesis consists of manuscripts that have been accepted or are under review. Chapter 3 includes a manuscript that investigates the optimization of the reflection coefficient of both the RIS-RGSSK and the RIS-RGSM schemes to improve the SE. Chapter 3 is in the form of a manuscript that has been accepted to *IEEE Wireless Communications Letters*.

Chapter 4 includes a manuscript that analyzes the performance of both the RIS-RGSSK and the RIS-RGSM schemes. Chapter 4 presents closed-form PEPs for both schemes. Chapter 4 is currently under review for publication.

Finally, Chapter 5 summarizes the main contributions of this thesis and explores potential research directions in light of these results.

References

[1] Y. Liu, X. Liu, X. Mu, T. Hou, J. Xu, M. Di Renzo, and N. Al-Dhahir, "Reconfigurable intelligent surfaces: Principles and opportunities," *IEEE Commun. Surv. Tutor.*, vol. 23, no. 3, pp. 1546–1577, Third Quarter 2021.

[2] E. Basar, M. Di Renzo, J. De Rosny, M. Debbah, M.-S. Alouini, and R. Zhang, "Wireless communications through reconfigurable intelligent surfaces," *IEEE Access*, vol. 7, pp. 116 753–116 773, 2019.

[3] X. Zhu, L. Yuan, Q. Li, L. Jin, X. Nie, C. Pan, and J. Zhang, "RIS-assisted full-duplex space shift keying: System scheme and performance analysis," *IEEE Trans. Green Commun. Netw.*, Jul. 2023.

[4] J. Li, S. Dang, M. Wen, Q. Li, Y. Chen, Y. Huang, and W. Shang, "Index modulation multiple access for 6G communications: Principles, applications, and challenges," *IEEE Netw.*, vol. 37, no. 1, pp. 52–60, Jan./Feb. 2023.

[5] E. Basar, M. Wen, R. Mesleh, M. Di Renzo, Y. Xiao, and H. Haas, "Index modulation techniques for next-generation wireless networks," *IEEE Access*, vol. 5, pp. 16 693–16 746, 2017.

2. Background

2.1 Overview of Reconfigurable Intelligent Surface (RIS)

2.1.1 Introduction to RIS

The concept of RIS comes as an evolution of past technologies, including passive reflectarrays and metasurfaces [1], [2]. Reflectarrays are also known as plane reflection antenna [1]. Its working principle is basically the same as that of a parabolic antenna. Metasurfaces, on the other hand, are planar structures made up of subwavelength meta-atoms arranged in a periodic pattern [1]. These artificial materials can manipulate and control electromagnetic (EM) waves by imparting desired phase shifts and amplitude modulation at subwavelength scales. RISs build upon the concepts of these technologies by adding reconfigurability and intelligence to the surfaces, allowing for dynamic control over how EM waves are reflected or scattered [1]. Compared with conventional relay, such as amplify-and-forward relay and decode-and-forward relay, passive RIS has no radio frequency (RF) chain and does not need extra energy to operate [3]. Due to the advancements in materials and electronics, RIS has born as an improved technology, making it suitable for modern wireless networks. RIS has become a prospective solution to the needs for enhancing performance in emerging 5th-generation (5G) and potentially 6th-generation (6G) wireless networks, offering new solutions for signal optimization and network efficiency [4], [5], [6]. In the literature, RIS is usually described as an innovative technology designed to enhance wireless communication systems by controlling EM properties of incident signals through an array of typically passive or quasi-passive elements. These elements can then vary the phase, amplitude and/or polarization in such a manner that enhances the received quality of these signals. The capability of channel control propagation of RIS makes it a key factor in its potential to revolutionize

future wireless systems [4], [7].

2.1.2 Operating Principle

A traditional RIS consists of a two-dimensional planar metasurface composed of numerous nearly-passive elements designed to reflect EM waves in a controlled manner by adjusting the amplitude and phase of these signals. RIS can be build using various technologies, such as liquid crystals [8], microelectromechanical systems [9], and electromechanical switches [10]. An RIS typically consists of three layers: a meta-atom layer with passive scattering elements, a control layer that manages the reflection properties of these elements through a smart controller, and a communication layer that interfaces with other network components such as base stations (BSs) and access points (APs) [5], [8], [11].

Most RIS implementations focus on nearly-passive elements that do not amplify the incident signals. Due to this, a nearly-passive RIS needs to be large to achieve the desired beamforming gain, as the path-loss increases with the distance between the transmitter, RIS, and receiver. To address size limitations and extend coverage, active or hybrid RIS options incorporate active RF components that can amplify signals. While both passive and active RIS operate on similar principles, active RIS requires additional power for signal amplification, making it more energy-consuming but potentially more effective for enhancing signal coverage [11], [12], [13]. A fair performance comparison between RIS and relay was conducted in [3], it was demonstrated that RIS not only achieved the same EE to half-duplex relay, but also was comparable to full-duplex relay in terms of the SE in [3].

2.1.3 Architecture of RIS

Traditionally, each RIS reflecting element is managed by a tunable circuit, which can be modeled as a tunable impedance linked to ground [14]. Building on this, two new circuit topologies were presented in [15], where all or some of the RIS reflecting elements are interconnected through a reconfigurable impedance network. Based on the connection configuration of the reflecting elements, RIS can be classified into three types of architecture:

- **Single connected RIS:** This is the conventional setup frequently discussed in the

literature, where each RIS reflecting element is individually controlled by a reconfigurable impedance connected to the ground. This architecture is the simplest among RIS designs [15]. We adopt this architecture for the schemes discussed in the later chapters of this thesis.

- **Fully connected RIS:** In this configuration, every RIS element is linked to all other reflecting elements via a reconfigurable impedance network. This setup enhances the RIS's received signal power due to increased degrees of freedom. However, this benefit is achieved at the expense of a more complex circuit topology [15].

- **Partially connected RIS:** As the number of reconfigurable impedance components increases, the practical application of fully connected RIS becomes challenging. Therefore, the partially connected RIS architecture provides a balance between complexity and performance by incorporating elements from both the single and fully connected RIS designs [15].

2.1.4 Classification of Smart Surfaces and the Role of RIS

The development of RIS is part of a larger trend in wireless communication technologies, where various types of smart surfaces have emerged. Understanding the broader landscape of these surfaces helps contextualize the specific role that RIS plays. In this subsection, we explore the key types of smart surfaces found in the literature, highlighting RIS features compared to other intelligent surfaces.

1. **Digitally Controllable Scatterers (DCSs)**
   DCSs are smart surfaces that emphasize digital control over local scatterers. These elements, often passive, cannot amplify signals and rely on mutual coupling for operation, resulting in high spatial correlation among unit cells. DCSs are closely related to RIS but with a focus on digital control [16].

2. **Large Intelligent Surfaces (LISs)**
   LISs are considered an advancement beyond massive multiple-input and multiple-

output (mMIMO) technology. These active surfaces feature individual antenna elements equipped with dedicated RF chains, power amplifiers, and signal processing capabilities, allowing for more sophisticated operations. Each unit element may have its own complete RF chain, making LISs highly versatile [16].

3. **RIS**

   RIS functions primarily as reflectors, with unit elements that can individually adjust their phase response for tasks such as beamsteering. Unlike LISs, RISs typically do not amplify incoming radio waves, focusing instead on modifying the phase response without altering amplitude [16].

4. **Software Controllable Surfaces (SCSs)**

   SCSs are smart surfaces managed and optimized through software-defined networking technologies. Equipped with nano-communication networks and low-power sensors for environmental monitoring, SCSs can perform local operations autonomously, though this may increase the complexity and power consumption of the surface [16].

2.1.5 Applications of RIS

RIS technology is utilized to enhance various aspects of wireless communications, including signal coverage, interference reduction, SE, and EE. Applications range from improving indoor coverage to optimizing network performance in urban environments and integrating with 5G and future networks to support high-speed, reliable connections [6], [13], [16]. Additionally, RIS can be integrated into existing network infrastructure, such as BSs and user equipment, without requiring significant changes. This integration can enhanced performance, reduced dead zones, and improved efficiency [6], [13], [16], [17].

For future wireless systems, the potential applications of RIS for enhancing communication can include:

1. **Immersive Communication:** RIS can support applications such as extended reality and ultra-high-definition video services, which rely on high-frequency, wideband signal

transmission. RIS helps overcome severe path loss and bypass obstacles by providing high beamforming gains and additional propagation paths [18].

2. **Dead Zone Coverage:** RIS elements can reflect wireless signals, providing coverage for dead zones in conventional terrestrial networks, thereby ensuring consistent and reliable connectivity even in challenging environments [19].

3. **Massive Communications:** In scenarios such as smart cities, environmental monitoring, and internet-of-things (IoT) applications, RIS can boost system throughput and fairness for densely deployed devices by optimizing reflections/refractions and integrating them with non-orthogonal multiple access (NOMA) schemes [20].

4. **Ubiquitous Connectivity:** RIS, when deployed massively and flexibly in strategic locations, can achieve ubiquitous connectivity even in complex environments with many scatterers and obstacles. It could also be installed on maritime or aerial platforms such as ships, unmanned aerial vehicles (UAVs), balloons, airships, and satellites to extend wireless coverage to scarcely covered or remote areas [21].

5. **Ultra-Reliable and Low Latency Communications (URLLC):** For critical applications such as industrial control, telemedicine, and emergency services, RIS could improve channel quality and transmission reliability by creating a dominant line-of-sight path, reducing multipath fading. In high-mobility scenarios such as autonomous driving, RIS can enhance signal strength either by being deployed onboard UAV to support the requirements of very high reliability and very low latency of URLLC [22].

2.2 Overview of Index Modulation (IM)

2.2.1 Introduction to IM

IM is an innovative technique designed to enhance the performance of wireless communication systems by encoding data into the indices of various resources, such as antennas, subcarriers, or time slots [23]. Unlike traditional modulation schemes, which encode information directly into signal amplitudes, phases, or frequencies, IM exploits the indices of

communication resources to convey additional information. This approach leverages the index of a resource to represent different data symbols, thereby expanding the data-carrying capacity of traditional communication systems [23].

The popularity of IM it is characterized by two main aspects: its basic principle and its role in future wireless systems. IM operates on the premise that each communication resource can be indexed, and these indices can be used to encode information. For instance, in a multiple-input and multiple-output (MIMO) system, different antennas can be assigned to indices, and the selection of these indices to transmit data can enhance system performance. Similarly, in orthogonal frequency-division multiplexing (OFDM) systems, subcarriers are indexed, and data can be encoded by selecting specific subcarriers [24], [23]. Hence, IM is well positioned to be a major technology in the advancement of wireless networks particularly with the introduction of 5G, and further on, which might potentially contribute to meet the increasing need for higher data rates and SE improvements through the use of new dimensions of the communication resources [25], [24].

2.2.2 Applications of IM

IM has a range of applications across different communication systems, each benefiting from its unique indexing techniques. Existing IM techniques are commonly classified into various signal domains, which include spatial-domain IM (SD-IM), channel-domain IM (CD-IM) scheme, time-domain IM (TD-IM), and frequency-domain IM (FD-IM) [26]. CD-IM is also known as media-based modulation (MBM). FD-IM is also referred to as OFDM with IM (IM-OFDM), where IM is performed on the orthogonal subcarriers. The SD-IM technique is also known as simply spatial modulation (SM). Depending on the signal domain, these applications may include the following:

1. **SD-IM scheme**

   The SD-IM scheme exploits the SD to convey information bits not only by the data symbols, but also by the antenna indexes activating/deactivating one or multiple antennas [24].

   Applications of SD-IM include the classical SM [27]. Here, the information bits are

conveyed by amplitude-phase modulation (APM) and the index of a single activated antenna. In the space shift keying (SSK), the information bits are only carried by the index of single activated transmit antenna without APM transmission [28]. Another application of SM is the generalized version of the SSK (GSSK), where information bits are carried by the indices of multiple activated transmit antenna without APM transmission, and the generalized SM (GSM) where information bits are carried by IM with APM transmission [29].

2. **CD-IM scheme**

The CD-IM scheme is a technique that enhances data transmission in RF communications by using special external components to alter the communication channel. In CD-IM, IM operations are not performed on the transmitter or receiver, such as antennas, subcarriers or time slots, but on the variable channel states by using tunable elements such as RF mirrors or electronic switches, which are typically placed close to the transmit antenna to modify the channel properties. By controlling the on-off status of these components, the system can generate multiple channel states, specifically $2^{m_{\mathrm{rf}}}$ states when m_{rf} RF mirrors are used. Here, each channel state corresponds to a different index. These indices are then used to convey additional bits of information [30].

For the CD-IM, applications include the differential MBM (DMBM), where differential coding is employed in single-input and multiple-output (SIMO) type MBM systems [31]. In the layered MIMO with MBM, index bits are conveyed by the indices of selected channel states in MIMO systems [32]. Another application of the CD-IM is the combination of GSM with MBM systems; here in the GSM-MBM, index bits are conveyed by the indices of selected channel states in GSM systems [33].

3. **TD-IM scheme**

IM can also be applied to time-division systems by modulating the indices of time slots. This method enhances data transmission rates and system performance by optimizing the use of available time slots, resulting in more efficient communications [34].

Examples of TD-IM include the single-carrier-based IM (SC-IM), where index bits

are conveyed by the indices of activated time slots [35]. Unlike in SC-IM, in the dual-mode SC-IM (DM-SCIM), all the time slots are activated, modulated by two different constellation alphabets [36]. Another application of the TD-IM is the faster-than-Nyquist rate IM (FTN-IM), where index bits are conveyed by indices of the activated time slots in the FTN-rate based single carrier system to reduce inter-symbol interference [37].

4. **FD-IM scheme**

   In OFDM systems, IM can be incorporated by modulating the indices of subcarriers. This technique enhances the SE by utilizing subcarriers more effectively, which can lead to higher data rates compared to traditional OFDM [38], [39], [40].

   Applications of IM-OFDM include the subcarrier index modulation with OFDM (SIM-OFDM) where activated subcarriers are determined by the corresponding majority bit-values of an on–off keying data stream [41]. Also, the enhanced subcarrier index modulation with OFDM (ESIM -OFDM), which activates only one subcarrier for each subcarrier pair to carry one index bit [42]. Additionally, in the generalized SIM-OFDM, for each subblock, multiple subcarriers are activated to convey index bits [43].

2.3 Literature Review

RISs offer significant potential for enhancing data rates in wireless networks by acting as passive reflectors that manipulate the phase of incident signals, thereby improving propagation conditions [1], [44]. To achieve these improvements, RIS can be integrated with other technologies such as multiple-input single-output (MISO), MIMO, OFDM, and, among others, IM.

2.3.1 RIS-assisted with MISO, MIMO and/or OFDM

In recent efforts to address the demand for high SE and improved EE, the work in [45] investigated the use of RIS in OFDM systems. The inherent trade-off between the SE and EE in OFDM systems presents a challenge, which researchers seek to overcome. To address this challenge, the authors in [45] developed a cooperative approach using RIS in

OFDM-IM systems with hybrid indexing. They introduced a frequency-dependent control mechanism for RIS and proposed to activate or deactivate RIS elements strategically. This strategy aimed to optimize the performance of OFDM-IM systems by improving the SE while maintaining EE. This work demonstrated that the proposed methodology successfully enhances both the SE and EE compared to traditional OFDM-IM systems. Notably, the solution compensates for a 0.5 SE loss in an OFDM-IM system with quadarture phase shift keying (QPSK) when compared to a traditional OFDM system. This improvement in the SE while maintaining EE showcases the effectiveness of the proposed hybrid indexing approach in cooperative RIS-aided OFDM-IM systems.

Moreover, the integration of RIS into cognitive radio (CR) networks has been proved to be effective for MISO systems. The work in [46] explored an RIS-assisted downlink MISO-CR system to improve both the SE and EE. The authors in [46] addressed this problem by proposing a maximization problem that involved jointly optimizing the beamforming at the secondary user's transmitter and the reflecting coefficients at each RIS to maximize the achievable rate of secondary users, while meeting power constraints at the secondary user's transmitter. The main findings in this work include SE improvement, allowing for increased data transmission over available bandwidth and better spectrum resource utilization. Additionally, optimizing beamforming at secondary user transmitters and reflecting coefficients at each RIS led to enhanced EE by minimizing energy consumption while maintaining or improving communication performance. However, the improvements in the SE and EE obtained in this work are based on comparisons with different scenarios or variations within the study itself.

RISs have also been explored within MIMO systems. Recent works demonstrated the potential of RIS in enhancing the SE of cell-free (CF) MIMO systems. The problem being considered in the work in [47] is how to improve the uplink performance of a CF-mMIMO system that is affected by hardware impairments. Specifically, the study focused on enhancing coverage quality, SE, and EE using RIS. To address this problem, the authors formulated an optimization problem that included optimizing large-scale fading decoding weights and power control coefficients to enhance the SE and ensure fairness among user equipments. The

proposed max-min SE algorithm, with a closed-form solution, iteratively optimized these key factors, balancing system parameters for improved SE and EE while considering user equipment fairness. Through simulations and theoretical analysis, they compared scenarios with varying numbers of APs versus RIS elements to evaluate the tradeoffs between using more APs or deploying more RISs, using more APs to increase spatial diversity and deploying more RISs led to improvements in the SE and EE.

The integration of RIS into multi-user millimeter-wave (mmWave) MIMO systems has been shown to significantly enhance the SE. The performance of a system aided by multiple RISs arranged in a circular layout was evaluated in [48]. The problem being considered in [48] is maximizing the SE and EE in multi-user MIMO OFDM systems with the integration of RIS and addressing hardware impairments. The authors in [48] addressed this problem by formulating a joint MIMO precoding and RIS optimization problem. They explored various RIS configurations such as regular, simultaneously transmit and reflect, and multi-sector beyond diagonal RIS to enhance system performance in multi-user MIMO OFDM broadcast channels. The main findings of this work indicate that RIS can significantly improve system performance even with a relatively low number of RIS elements.

In their research, the authors in [49] also incorporated RIS to a MIMO system to improve the SE. The problem being considered in [49] is improving the SE in wireless communication systems, specifically focusing on joint beamforming design for BS and beyond-diagonal RIS. The authors addressed the problem by using deep reinforcement learning to jointly optimize the phase shift matrix of RIS elements and BS beamforming. They also optimized the position of non-diagonal elements in the RIS phase shift matrix to maximize the SE. The main findings include that the proposed beyond-diagonal RIS architecture with deep reinforcement learning outperforms traditional diagonal RIS setups in terms of SE. Additionally, there is a trade-off between accuracy and complexity based on varying quantization bits used by deep reinforcement learning algorithms.

2.3.2 RIS-assisted Systems with IM

Foundational models such as RIS-SSK and RIS-SM have been proposed in [50], where RIS components are utilized as part of the transmitter while receive antennas implement IM, effectively increasing the SE [50]. The problem being considered in [50] is how to enhance the SE at extremely low SNR. The focus is on utilizing RIS to improve the reception of incoming signals and increase spectral efficiency without relying on complex massive MIMO systems. In the work of [50], the RIS-SSK scheme conveys information bits through a single selected receive antenna index using IM, while RIS-SM uses IM selection along with additional bits through ordinary M-ary modulation. To address this problem, the authors opted for maximizing the SNR value at the selected receive antenna. The authors in [50] also formulated maximum energy-based suboptimal detectors as well as exhaustive search-based optimal detectors for these schemes. Additionally, a unified framework was presented to derive theoretical average bit error probability. Computer simulations further confirmed the potential of RIS-assisted IM techniques to enhance wireless communication systems beyond conventional MIMO solutions.

After the RIS-SM and RIS-SSK initiatives, the authors in [51] presented the integration of time IM (TIM) with RIS-aided receive antenna selection, with the purpose of enhancing both the SE and bit error rate (BER) performance. By leveraging the TD and SD, the TIM-RIS-receive-antenna design encoded additional index information through the indexes of time index (TI) vectors and receive antennas. The methodology involved selecting a TI vector from a predefined set based on the TI information to modulate quadrature amplitude modulation/phase-shift keying (QAM/PSK) symbols, resulting in a TI vector symbol. This symbol, containing both zero and non-zero elements, facilitated the combination of TIM with receive antennas to support RIS-SM and RIS-SSK. Simulation results showed that TIM-RIS receive-antenna significantly enhances BER performance compared with traditional RIS-aided systems like RIS-SM.

Furthermore, a proposed RIS-based reflection pattern modulation (RIS-RPM) scheme has been proposed in [52], where a subset of reflecting elements is switched to on state to

achieve efficient beamforming. The problem considered in [52] is enhancing signal quality by jointly optimizing active beamforming at the AP and passive beamforming at the RIS through RPM techniques. The authors in [52] formulated an optimization problem to maximize the average received signal power by jointly optimizing digital beamforming at the AP and analog beamforming at the RIS, accounting for channel state information errors. The activation of reflecting elements is determined by the information to be transmitted, aiming to maximize the SNR at the receiver in both active and passive beamforming scenarios. This study includes examining joint active and passive beamforming and computing the communication outage probability to optimize the system's performance. This work demonstrated that integrating RPM into joint active-passive beamforming design leads to significant improvements in achievable rate compared to conventional RIS-assisted system such as RIS-SSK.

Another case of combination of RIS-assited systems with RM is the joint mapped RM (JRM) presented in [53]. The problem being considered in [53] is how to reliably transmit information using RIS to enhance transmission reliability. The JRM uses the on-off states of RIS elements to carry information bits. When a portion of the RIS elements is always turned off, the on-off states-based reflection modulation reduces the large-scale aperture gain of the RIS. This RM scheme activates all elements to achieve the maximum diversity gain, and the index of a reflection coefficient pattern is utilized to convey additional information bits. Here, the sets of active signals and reflecting patterns are designed in both separate and joint manners, and the index of a reflection pattern conveys the passive information per channel use. The authors addressed the problem by proposing a discrete optimization-based joint signal mapping, shaping, and reflecting design for the JRM. This optimization minimizes the BER by considering a given transmit signal candidate set, and a given reflecting pattern candidate set. By optimizing these parameters together, they were able to significantly improve system performance in high SNR conditions compared to existing designs. The authors reported that their proposed scheme outperformed the RIS-SM by around $4 - 5$ dB in the depicted high SNR regime.

Following the RM principle, the work in [54] proposed the RIS-aided quadrature RM

(RIS-QRM) scheme to enhance information transmission in RIS-aided downlink MISO wireless systems. The focus in [54] was to improve the system performance by optimizing the use of RIS without relying solely on on-off states of RIS elements, which can lead to power loss. The concept of SM has also been applied within the RIS entity in [54] in order to transmit additional data bits. In [54], RIS is divided into two subsets to reflect signals in two orthogonal directions (in phase (I) and quadrature (Q) signal components), and the indices of the subsets represent the transmitted information of RIS. Then, a maximum likelihood (ML) detector is applied at the receiver to recover the transmitted information of RIS. The authors in [54] proposed an optimization problem to maximize the received SNR while jointly optimizing two key components: the phases of the RIS and active beamforming at the AP. The authors in [54] used maximum-ratio transmission as transmit beamforming technique to solve their optimization problem. The reported results in [54] showed that the RIS-QRM effectively partitions RIS elements to reflect incident signals towards two orthogonal directions, enhancing reflection power utilization, achieving 4.0 dB improvement than the RIS-RPM at high SNRs. In addition, analytical and simulation results demonstrate that RIS-QRM improves error performance for additional data bits without compromising the error performance of modulated bits compared to existing on-off-based schemes.

Building on the RIS principle, recent advancements have incorporated generalized approaches within RIS and IM to enhance the SE. The use of the generalized concept within RIS-assisted systems is presented in [55] with the joint RIS grouping design assisted generalized quadrature RM (JGD-GQRM). The authors in [55] proposed an algorithm for spatially grouping a limited number of RIS elements. This approach enables the use of grouped redundant reflection patterns, which are then jointly mapped with constellation symbols, to improve BER. The JGD-GQRM scheme incorporated full reflection passive beamforming to further boost the SE. Additionally, a low-complexity sequential GD method was presented to reduce the complexity while achieving BER performance close to that of optimal detectors. The authors in [55] reported a 2.5 dB improvement of the RIS-JGD-GQRM compared to the RIS-JRM, while transmitting the same number of information bits.

In the work found in [56], the authors explored advanced SM techniques integrated with

RIS to enhance the SE and EE for future wireless networks. They presented the dual-hop RIS-based SM (DH RIS-SM) scheme and an enhanced SM (RIS-ESM) technique. The RIS-ESM scheme, incorporating primary and secondary modulations, significantly improved the SE by conveying information through both the indexes of active antennas and constellations transmitted from each antenna. The authors in [56] addressed the RIS phase optimization of the DH RIS-SM via the maximization of the received SNR at the receiver as the problem presented in [57]. The results reported 45% improvement in the SE of the RIS-ESM compared to the DH RIS-SM technique while maintaining comparable BER performance.

Other recent proposals include schemes such as the RIS-assisted receive quadrature SSK (RIS-RQSSK) and RIS-assisted receive QSM (RIS-RQSM) [58], [59]. The main problem addressed in these works is to enhance the efficiency of wireless communication systems using RIS in order to improve the SE and error rate performance. These schemes aimed to optimize the SNR of the real and imaginary parts of signals at different antennas, thereby enhancing the SE without significant SNR degradation. The authors in [58], [59] addressed this problem by proposing a low-complexity GD at the receiver to determine maximum energy per dimension, along with defining a max-min optimization problem based on Lagrange duality to maximize received SNR ratio components. Additionally, they derived analytical solutions that simplified multi-variable optimization into solving a single-variable equation for simpler design implementation. The authors in [58], [59] reported that the proposed RIS-RQSSK system achieves 3.5 dB performance improvement over the RIS-SM scheme [58], and the RIS-RQSM system achieves approximately 7 dB performance improvement over the RIS-SM system [59]. However, both the RIS-RQSSK and RIS-RQSM activate only two antennas, which limit their SE. RIS-RQSSK can only transmit one extra bit per antenna, while RIS-RQSM, despite using M-ary modulation, is also limited to the activation of only two receive antennas.

2.3.3 RIS-assisted Implementations

Several innovative RIS prototypes and field trials have demonstrated significant improvements in wireless communication across various frequency bands. Notable developments

include a programmable metasurface-based 8-PSK transmitter operating at the 4.25 GHz band presented in [60], and a 3200-element RIS at 2.4 GHz that significantly enhanced signal strength [61]. Additionally, a 36-element antenna array at 2.4 GHz improved channel capacity was developed in [62]. In addition, the authors in [63] presented an experimental study that demonstrates the practical implementation of RIS in cooperative communication scenarios, showcasing substantial data rate improvements. Particularly, a RIS prototype designed for mmWave frequencies was presented. This prototype includes modular hardware components such as hosts for parameter setting and data exchange, universal software radio peripherals, and a RIS with 256 two-bit elements. The system in [63] was used to build a holographic MIMO surface-aided wireless communication prototype, integrating flexible software for source and channel coding and OFDM modulation. Measurement results reported antenna gains of 21.7 dBi at 2.3 GHz and 19.1 dBi at 28.5 GHz, confirming its capability to enhance wireless communication systems.

Other experiments have also been conducted, such as a 1100-element RIS prototype at 5.8 GHz that achieved high performance across various scenarios in [64]. The authors in [64] proposed an algorithm for configuring the RIS, which leverages geometrical array properties and a practical feedback link between the receiver and the RIS. Through extensive indoor and outdoor field trials, this study reported significant performance, achieving a 26 dB power gain in an indoor scenario with a concrete wall obstruction and a 27 dB gain in outdoor measurements. Additionally, the system successfully transmitted a 32 Mbps data stream over a distance of 500 meters, showcasing the RIS's potential to enhance wireless communication systems significantly. Furthermore, field trials demonstrated remarkable improvements, including a 40 dB increase in indoor received power in the sub-6 GHz band [65], and enhanced throughput in a 5G mmWave commercial network at 27 GHz in [66].

References

[1] M. Di Renzo, A. Zappone, M. Debbah, M.-S. Alouini, C. Yuen, J. de Rosny, and S. Tretyakov, "Smart radio environments empowered by reconfigurable intelligent surfaces: How it works, state of research, and the road ahead," *IEEE J. Sel. Areas Commun.*, vol. 38, no. 11, pp. 2450–2525, Nov. 2020.

[2] Q. Wu and R. Zhang, "Towards smart and reconfigurable environment: Intelligent reflecting surface aided wireless network," *IEEE Commun. Mag.*, vol. 58, no. 1, pp. 106–112, Jan. 2019.

[3] Q. Gu, D. Wu, X. Su, J. Jin, Y. Yuan, and J. Wang, "Performance comparisons between reconfigurable intelligent surface and full/half-duplex relays," in *Proc. IEEE 94th Veh. Technol. Conf.*, 2021, pp. 01–06.

[4] L. Li, Y. Shuang, Q. Ma, H. Li, H. Zhao, M. Wei, C. Liu, C. Hao, C.-W. Qiu, and T. J. Cui, "Intelligent metasurface imager and recognizer," *Light, Sci. Appl.*, vol. 8, no. 1, pp. 1–9, Dec. 2019.

[5] Z. Wang, L. Liu, S. Zhang, and S. Cui, "Massive MIMO communication with intelligent reflecting surface," *IEEE Trans. Wirel. Commun.*, vol. 22, no. 4, pp. 2566–2582, Apr. 2023.

[6] W. Tang, M. Z. Chen, Y. Zeng, L. Liang, K. H. Wong, and S. Jin, "Wireless communications with reconfigurable intelligent surface: Path loss modeling and experimental measurement," *IEEE Trans. Wireless Commun.*, vol. 20, no. 1, pp. 421–439, Jan. 2020.

[7] M. A. ElMossallamy, H. Zhang, L. Song, K. G. Seddik, Z. Han, and G. Y. Li, "Reconfigurable intelligent surfaces for wireless communications: Principles, challenges, and opportunities," *IEEE Trans. Cogn. Commun. Netw.*, vol. 6, no. 3, pp. 990–1002, Sep. 2020.

[8] E. Basar, M. Di Renzo, J. De Rosny, M. Debbah, M.-S. Alouini, and R. Zhang, "Wireless communications through reconfigurable intelligent surfaces," *IEEE Access*, vol. 7, pp. 116 753–116 773, 2019.

[9] X. Cheng, Y. Lin, W. Shi, J. Li, C. Pan, F. Shu, Y. Wu, and J. Wang, "Joint optimization for ris-assisted wireless communications: From physical and electromagnetic perspectives," *IEEE Trans. Commun.*, vol. 70, no. 1, pp. 606–620, Jan. 2021.

[10] K. Qu, K. Chen, J. Zhao, N. Zhang, Q. Hu, J. Zhao, T. Jiang, and Y. Feng, "An electromechanically reconfigurable intelligent surface for enhancing sub-6g wireless communication signal," *J. Inf. Intell.*, vol. 1, no. 3, pp. 207–216, 2023.

[11] T. J. Cui, S. Liu, and L. Zhang, "Information metamaterials and metasurfaces," *J. Mater. Chem. C*, vol. 5, no. 15, pp. 3644–3668, Mar. 2017.

[12] C. Huang, A. Zappone, G. C. Alexandropoulos, M. Debbah, and C. Yuen, "Reconfigurable intelligent surfaces for energy efficiency in wireless communication," *IEEE Trans. Wirel. Commun.*, vol. 18, no. 8, pp. 4157–4170, Aug. 2019.

[13] S. Zhang and R. Zhang, "Intelligent reflecting surface aided multi-user communications: Capacity region and deployment strategy," *IEEE Trans. Commun.*, vol. 69, no. 2, pp. 596–609, Feb. 2020.

[14] S. Abeywickrama, R. Zhang, Q. Wu, and C. Yuen, "Intelligent reflecting surface: Practical phase shift model and beamforming optimization," *IEEE Trans. Commun.*, vol. 68, no. 9, pp. 5849–5863, Sep. 2020.

[15] S. Shen, B. Clerckx, and R. Murch, "Modeling and architecture design of reconfigurable intelligent surfaces using scattering parameter network analysis," *IEEE Trans. Wirel. Commun.*, vol. 21, no. 2, pp. 1229–1243, Nov. 2021.

[16] M. Di Renzo, A. Zappone, M. Debbah, M.-S. Alouini, C. Yuen, J. De Rosny, and S. Tretyakov, "Smart radio environments empowered by reconfigurable intelligent surfaces: How it works, state of research, and the road ahead," *IEEE J. Sel. Areas Commun.*, vol. 38, no. 11, pp. 2450–2525, Nov. 2020.

[17] Ö. T. Demir and E. Björnson, "Is channel estimation necessary to select phase-shifts for RIS-assisted massive MIMO?" *IEEE Trans. Wirel. Commun.*, vol. 21, no. 11, pp. 9537–9552, Nov. 2022.

[18] G. Chen, Q. Wu, W. Chen, Y. Hou, M. Jian, S. Zhang, J. Li, and L. Hanzo, "Intelligent reflecting surface aided MIMO networks: Distributed or centralized architecture?" *arXiv.org*, Oct. 2023.

[19] S. Zhang, H. Zhang, B. Di, Y. Tan, M. Di Renzo, Z. Han, H. Vincent Poor, and L. Song, "Intelligent omni-surfaces: Ubiquitous wireless transmission by reflective-refractive metasurfaces," *IEEE Trans. Wirel. Commun.*, vol. 21, no. 1, pp. 219–233, Jan. 2022.

[20] G. Yang, X. Xu, Y.-C. Liang, and M. D. Renzo, "Reconfigurable intelligent surface-assisted non-orthogonal multiple access," *IEEE Trans. Wirel. Commun.*, vol. 20, no. 5, pp. 3137–3151, May 2021.

[21] Q. Wu, J. Xu, Y. Zeng, D. W. K. Ng, N. Al-Dhahir, R. Schober, and A. L. Swindlehurst, "A comprehensive overview on 5G-and-beyond networks with UAVs: From communications to sensing and intelligence," *IEEE J. Sel. Areas Commun.*, vol. 39, no. 10, pp. 2912–2945, Oct. 2021.

[22] Z. Huang, B. Zheng, and R. Zhang, "Transforming fading channel from fast to slow: Intelligent refracting surface aided high-mobility communication," *IEEE Trans. Wirel. Commun.*, vol. 21, no. 7, pp. 4989–5003, Jul. 2022.

[23] T. Mao, Q. Wang, Z. Wang, and S. Chen, "Novel index modulation techniques: A survey," *IEEE Commun. Surv. Tutor.*, vol. 21, no. 1, pp. 315–348, 1st Quart. 2019.

[24] E. Basar, M. Wen, R. Mesleh, M. Di Renzo, Y. Xiao, and H. Haas, "Index modulation techniques for next-generation wireless networks," *IEEE Access*, vol. 5, pp. 16 693–16 746, 2017.

[25] S. D. Tusha, A. Tusha, E. Basar, and H. Arslan, "Multidimensional index modulation

for 5G and beyond wireless networks," *Proc. IEEE*, vol. 109, no. 2, pp. 170–199, Feb. 2021.

[26] E. Basar, "Index modulation techniques for 5G wireless networks," *IEEE Commun. Mag.*, vol. 54, no. 7, pp. 168–175, Jul. 2016.

[27] S. Ganesan, R. Mesleh, H. Ho, C. W. Ahn, and S. Yun, "On the performance of spatial modulation OFDM," in *2006 Fortieth Asilomar Conference on Signals, Systems and Computers*. IEEE, 2006, pp. 1825–1829.

[28] Y. A. Chau and S.-H. Yu, "Space modulation on wireless fading channels," in *IEEE 54th Vehicular Technology Conference. VTC Fall 2001. Proceedings (Cat. No. 01CH37211)*, vol. 3. IEEE, 2001, pp. 1668–1671.

[29] J. Jeganathan, A. Ghrayeb, and L. Szczecinski, "Generalized space shift keying modulation for MIMO channels," in *2008 IEEE 19th International Symposium on Personal, Indoor and Mobile Radio Communications*, 2008, pp. 1–5.

[30] S. Doğan Tusha, A. Tusha, E. Basar, and H. Arslan, "Multidimensional index modulation for 5G and beyond wireless networks," *Proce. IEEE*, vol. 109, no. 2, pp. 170–199, Feb. 2021.

[31] Y. Naresh and A. Chockalingam, "A low-complexity maximum-likelihood detector for differential media-based modulation," *IEEE Commun. Mag.*, vol. 21, no. 10, pp. 2158–2161, Oct. 2017.

[32] E. Seifi, M. Atamanesh, and A. K. Khandani, "Media-based MIMO: Outperforming known limits in wireless," in *2016 IEEE International Conference on Communications (ICC)*. IEEE, 2016, pp. 1–7.

[33] Y. Naresh and A. Chockalingam, "On media-based modulation using RF mirrors," *IEEE Trans. Veh. Technol.*, vol. 66, no. 6, pp. 4967–4983, Jun. 2017.

[34] S. Sugiura, T. Ishihara, and M. Nakao, "State-of-the-art design of index modulation in the space, time, and frequency domains: Benefits and fundamental limitations," *IEEE Access*, vol. 5, pp. 21 774–21 790, 2017.

[35] M. Nakao, T. Ishihara, and S. Sugiura, "Single-carrier frequency-domain equalization with index modulation," *IEEE Commun. Lett.*, vol. 21, no. 2, pp. 298–301, Feb. 2017.

[36] ——, "Dual-mode time-domain index modulation for Nyquist-criterion and faster-than-Nyquist single-carrier transmissions," *IEEE Access*, vol. 5, pp. 27 659–27 667, 2017.

[37] T. Ishihara and S. Sugiura, "Faster-than-Nyquist signaling with index modulation," *IEEE Wireless Commun. Lett.*, vol. 6, no. 5, pp. 630–633, Oct. 2017.

[38] G. Huang, Y. Ding, S. Ouyang, and V. Fusco, "Index modulation for OFDM RadCom systems," *J. Eng.*, vol. 2021, no. 2, pp. 61–72, Dec. 2020.

[39] S. Gao, M. Zhang, and X. Cheng, "Precoded index modulation for multi-input multi-output OFDM," *IEEE Trans. Wirel. Commun.*, vol. 17, no. 1, pp. 17–28, Jan. 2018.

[40] L. Zhang, A. Ijaz, P. Xiao, M. M. Molu, and R. Tafazolli, "Filtered OFDM systems, algorithms, and performance analysis for 5G and beyond," *IEEE Trans. Commun.*, vol. 66, no. 3, pp. 1205–1218, Mar. 2018.

[41] R. Abu-Alhiga and H. Haas, "Subcarrier-index modulation OFDM," in *2009 IEEE 20th International Symposium on Personal, Indoor and Mobile Radio Communications*. IEEE, 2009, pp. 177–181.

[42] D. Tsonev, S. Sinanovic, and H. Haas, "Enhanced subcarrier index modulation (SIM) OFDM," in *2011 IEEE GLOBECOM Workshops (GC Wkshps)*. IEEE, 2011, pp. 728–732.

[43] E. Başar, Ü. Aygölü, E. Panayırcı, and H. V. Poor, "Orthogonal frequency division multiplexing with index modulation," *IEEE Trans. Signal Process.*, vol. 61, no. 22, pp. 5536–5549, Nov. 2013.

[44] E. Basar, M. Di Renzo, J. De Rosny, M. Debbah, M.-S. Alouini, and R. Zhang, "Wireless communications through reconfigurable intelligent surfaces," *IEEE Access*, vol. 7, pp. 116 753–116 773, 2019.

[45] A. A. T, L. T, and M. T, "Spectral efficiency improvement in cooperative RIS aided OFDM-IM system with hybrid indexing," *Phys. Commun.*, vol. 66, p. 102398, May. 2024.

[46] J. Yuan, Y.-C. Liang, J. Joung, G. Feng, and E. G. Larsson, "Intelligent reflecting surface-assisted cognitive radio system," *IEEE Trans. Commun.*, vol. 69, no. 1, pp. 675–687, Jan. 2021.

[47] Y. Zhang, H. Zhao, W. Xia, W. Xu, C. Tang, and H. Zhu, "How much does reconfigurable intelligent surface improve cell-free massive MIMO uplink with hardware impairments?" *IEEE Trans. Commun.*, vol. 71, no. 11, pp. 1–1, Nov. 2023.

[48] M. Soleymani, I. Santamaria, A. Sezgin, and E. Jorswieck, "Maximizing spectral and energy efficiency in multi-user MIMO OFDM systems with RIS and hardware impairment," *arXiv.org*, 2024.

[49] S. Sobhi-Givi, M. Nouri, H. Behroozi, and Z. Ding, "Joint BS and beyond diagonal RIS beamforming design with DRL methods for mmWave 6G mobile communications," in *2024 IEEE WCNC.* IEEE, 2024, pp. 1–6.

[50] C.-X. Wang, F. Haider, X. Gao, X.-H. You, Y. Yang, D. Yuan, H. M. Aggoune, H. Haas, S. Fletcher, and E. Hepsaydir, "Cellular architecture and key technologies for 5G wireless communication networks," *IEEE Commun. Mag.*, vol. 52, no. 2, pp. 122–130, Feb. 2014.

[51] F. Huang, G. Wu, and X. Wang, "Joint time index modulation and receive antenna selection for RIS-aided communications," *IEEE Access*, vol. 11, pp. 111 692–111 700, 2023.

[52] S. Lin, B. Zheng, G. C. Alexandropoulos, M. Wen, M. D. Renzo, and F. Chen, "Reconfigurable intelligent surfaces with reflection pattern modulation: Beamforming design and performance analysis," *IEEE Trans. Wirel. Commun.*, vol. 20, no. 2, pp. 741–754, Feb. 2021.

[53] S. Guo, S. Lv, H. Zhang, J. Ye, and P. Zhang, "Reflecting modulation," *IEEE J. Sel. Areas Commun.*, vol. 38, no. 11, pp. 2548–2561, Nov. 2020.

[54] S. Lin, F. Chen, M. Wen, Y. Feng, and M. Di Renzo, "Reconfigurable intelligent surface-aided quadrature reflection modulation for simultaneous passive beamforming and information transfer," *IEEE Trans. Wirel. Commun.*, vol. 21, no. 3, pp. 1469–1481, Mar. 2022.

[55] X. Jin, X. Li, Y. Feng, M. Wen, and Y. Yao, "Joint RIS grouping design assisted generalized quadrature reflection modulation," *IEEE Trans. Veh. Technol.*, vol. 72, no. 4, pp. 5447–5451, Apr. 2023.

[56] S. H. Yasin, O. A. Omer, A. M. Nor, O. Fratu, S. Halunga, and A. S. Mubarak, "Reconfigurable intelligent surfaces-assisted enhanced spatial modulation for future wireless networks," *IEEE Access*, vol. 11, pp. 142 652–142 662, 2023.

[57] E. Basar, "Reconfigurable intelligent surface-based index modulation: A new beyond MIMO paradigm for 6G," *IEEE Trans. Commun.*, vol. 68, no. 5, pp. 3187–3196, May 2020.

[58] M. H. Dinan, N. S. Perović, and M. F. Flanagan, "RIS-assisted receive quadrature space-shift keying: A new paradigm and performance analysis," *IEEE Trans. Commun.*, vol. 70, no. 10, pp. 6874–6889, Oct. 2022.

[59] M. H. Dinan, M. Di Renzo, and M. F. Flanagan, "RIS-assisted receive quadrature spatial modulation with low-complexity greedy detection," *IEEE Trans. Commun.*, vol. 71, no. 11, pp. 1–1, Nov. 2023.

[60] W. Tang, J. Y. Dai, M. Chen, X. Li, Q. Cheng, S. Jin, K.-K. Wong, and T. J. Cui, "Programmable metasurface-based RF chain-free 8PSK wireless transmitter," *Electron. Lett.*, vol. 55, no. 7, pp. 417–420, Apr. 2019.

[61] V. Arun and H. Balakrishnan, "RFocus: Beamforming using thousands of passive antennas," in *17th USENIX symposium on networked systems design and implementation (NSDI 20)*, 2020, pp. 1047–1061.

[62] Z. Li, Y. Xie, L. Shangguan, R. I. Zelaya, J. Gummeson, W. Hu, and K. Jamieson, "Programmable radio environments with large arrays of inexpensive antennas," *GetMobile: Mobile Computing and Communications*, vol. 23, no. 3, pp. 23–27, 2020.

[63] L. Dai, B. Wang, M. Wang, X. Yang, J. Tan, S. Bi, S. Xu, F. Yang, Z. Chen, M. Di Renzo *et al.*, "Reconfigurable intelligent surface-based wireless communications: Antenna design, prototyping, and experimental results," *IEEE Access*, vol. 8, pp. 45 913–45 923, 2020.

[64] X. Pei, H. Yin, L. Tan, L. Cao, Z. Li, K. Wang, K. Zhang, and E. Björnson, "RIS-aided wireless communications: Prototyping, adaptive beamforming, and indoor/outdoor field trials," *IEEE Trans. Commun.*, vol. 69, no. 12, pp. 8627–8640, Dec. 2021.

[65] J. Rains, A. Tukmanov, T. J. Cui, L. Zhang, Q. H. Abbasi, M. A. Imran *et al.*, "High-resolution programmable scattering for wireless coverage enhancement: an indoor field trial campaign," *IEEE Trans. Antennas Propag.*, vol. 71, no. 1, pp. 518–530, Jan. 2023.

[66] H. Yang, S. Kim, H. Kim, S. Bang, Y. Kim, S. Kim, K. Park, D. Kwon, and J. Oh, "Beyond limitations of 5G with RIS: Field trial in a commercial network, recent advances, and future directions," *IEEE Commun. Mag.*, Dec. 2023.

3. RIS-Assisted Receive Generalized Space Shift Keying and Receive Generalized Spatial Modulation

Published as:

P. A. Marín, M. Hanif, and E. Bedeer, "RIS-assisted receive generalized space shift keying and receive generalized spatial modulation," *IEEE Wireless Commun. Lett.*, vol. 13, no. 10, pp. 2712–2716, Aug. 2024.

This chapter contains the manuscript of the paper which has been published in *IEEE Wireless Communication Letters*. In this paper, we introduce two novel RIS-assisted schemes: RIS-RGSSK and RIS-RGSM, designed to enhance wireless communication systems by utilizing reconfigurable intelligent surfaces (RIS) and index modulation (IM). The RIS-RGSSK scheme conveys information bits through the selection of multiple receive antennas, while the RIS-RGSM extends this by embedding information bits in the phase of the received signals using M-ary PSK modulation. We propose and solve an optimization problem for the RIS-RGSSK, which optimizes the phase shift of the RIS reflecting element to maximize the minimum values of the real component of the received signal. Our RIS-RGSSK optimal solution is extended to the RIS-RGSM scheme. Furthermore, we compare our results to another RIS-based system from the literature, showing the advantages of our proposed methods.

RIS-Assisted Receive Generalized Space Shift Keying and Receive Generalized Spatial Modulation

Porfirio A. Marín, Muhammad Hanif, and Ebrahim Bedeer

Abstract

In this paper, we enhance the performance of wireless communication systems by utilizing reconfigurable intelligent surface (RIS) and index modulation (IM). In particular, we introduce two schemes: RIS-assisted receive generalized space-shift keying (RIS-RGSSK) and RIS-assisted receive generalized spatial modulation (RIS-RGSM). In the RIS-RGSSK scheme, information bits are conveyed through selection of *multiple receive antennas*. The RIS-RGSM scheme takes RIS-RGSSK a step further by conveying information bits not only through the selection of *multiple receive antennas*, but also through embedding information bits in the phase of the received signals using M-ary phase shift keying (PSK) modulation. We also present simple yet efficient greedy detectors (GDs) for non-coherent detection of both schemes. Simulation results demonstrate the advantages of our proposed methods over existing schemes such as the RIS-assisted receive quadrature space-shift keying (RIS-RQSSK).

Keywords

Receive generalized space-shift keying (RGSSK), receive generalized spatial modulation (RGSM), RIS.

3.1 Introduction

To meet the growing data rate demands, researchers explore technologies to control the propagation channel, leading to the popularity of reconfigurable intelligent surface (RIS) as a potential approach for future wireless communications [1]. Recently, RIS garnered attention from both academia and industry as a candidate solution to improve the spectrum utilization and energy efficiency (EE) [1], [2], [3]. Another paradigm that is gaining interest in advancing communication systems is index modulation (IM) [4]. With IM schemes, the transmission of information bits occurs by activating or deactivating transmission/reception entities, including transmit antennas, receive antennas, and/or subcarriers, among others.

This introduces new dimensions for efficient information conveyance, potentially enhancing spectral efficiency (SE), while deactivating entities results in less power consumption while carrying extra information bits, which improves the EE of IM systems [4].

To obtain the benefits of IM in RIS-assisted systems, the authors in [5] proposed the RIS-assisted space shift keying (RIS-SSK), which makes real-time adjustments to the RIS for maximizing the instantaneous signal-to-noise-ratio (SNR) at *one receive antenna*. Following this, in [6] and [7], the spatial modulation (SM) principle is applied to a RIS-based system to transmit additional information bits utilizing the on-off stated of the RIS. In [8], a RIS-based receive antenna space-shift keying (RIS-RSSK) and a RIS-based receive spatial modulation (RIS-RSM) are introduced. The RIS-RSSK conveys information bits through *a single selected receive antenna* index using IM, while RIS-RSM uses IM selection along with additional bits through ordinary M-ary modulation. However, both schemes can only activate *one receive antenna* per IM symbol. The idea in [8] is extended in [9] with the introduction of the RIS-assisted receive quadrature space-shift keying (RIS-RQSSK), allowing the selection of *two receive antennas* independently in the real and imaginary dimensions. While RIS-RQSSK in [9] can also transmit extra bits, it is limited to transmitting only *one extra information bit per each of the only two antennas that can be selected*. In [10], the RIS-assisted receive quadrature spatial modulation (RIS-RQSM) scheme uses *two activated antenna indices* to convey spatial bits, and it transmits additional bits through ordinary M-ary modulation.

In this paper, inspired by the works in [8], [9], we present a RIS-assisted receive generalized space-shift keying (RIS-RGSSK), which operates based on the principle of generalized space-shift keying (GSSK), wherein *multiple antennas are chosen at the receiver*. Additionally, we present a RIS-assisted receive generalized spatial modulation (RIS-RGSM) scheme, where not only information bits are conveyed through the indexes of selected *multiple receive antennas*, but additional information bits are also conveyed via the received signal phase (i.e., using M-ary phase shift keying (PSK) modulation) at each selected antenna. The proposed RIS-RGSSK system optimizes the phase shift of the RIS reflecting elements to maximize the minimum value of the real part of the received signals at all the selected antennas. We choose the real part of the received signal instead of its squared absolute value (or, equivalently,

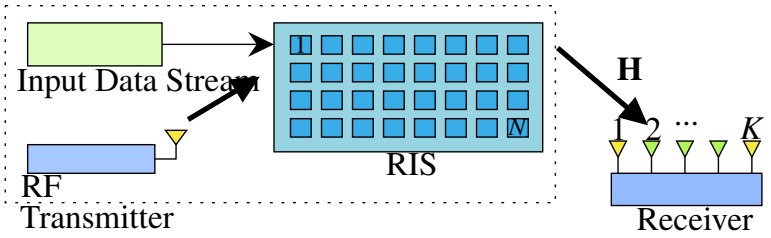

Figure 3.1: A schematic of the proposed RIS-RGSSK system.

the SNR) as in [8], [9] because it allows us to embed extra information in the phase of the transmitted signal in the proposed RIS-RGSM scheme. We also present non-coherent greedy detectors (GDs) for both schemes. Simulation results quantify the tradeoff between the SE and error rate performance of the proposed schemes when compared to competing schemes from the literature.

The paper proceeds as follows: Section II details the RIS-RGSSK and RIS-RGSM systems model. In Section III, we formulate and solve optimization problems for both schemes. Section IV includes simulations, and comparisons with a benchmark scheme. Finally, Section V concludes the paper.

3.2 System Model

This section presents the system model used in the paper. We utilize the RIS as an access point to convey information through the phases of its N reflecting elements to a receiver equipped with K antennas. The RIS elements reflect the incident waves from a nearby RF source. The phases of the reflected waves are controlled by an RIS controller, which receives information bits as an input as shown in Fig. 3.1.

We denote the baseband complex channel gains between the RIS elements and the kth receive antenna by $\mathbf{h}_k = \begin{bmatrix} h_{k,1}, & h_{k,2}, & \cdots, & h_{k,N} \end{bmatrix}$, where $k = 1, 2, \cdots, K$. The baseband receive signal at the kth receive antenna is

$$y_k = \sqrt{E_s}\mathbf{h}_k\boldsymbol{\theta} + n_k, \tag{3.1}$$

where E_s is the energy of the RF waves reflected by each RIS element per IM symbol, n_k denotes the additive white Gaussian noise at the kth receive antenna having zero mean and

variance of σ^2, and $\boldsymbol{\theta}$ is the N-dimensional complex vector, whose ith entry, θ_i, represents the reflection coefficient of the ith reflecting element for $i = 1, 2, \cdots, N$. In this work, we assume lossless reflection from the RIS elements, i.e., $|\theta_i| = 1$ for $i = 1, 2, \cdots, N$.

In the proposed RIS-RGSSK scheme, a total of L receive antennas are selected to convey the information bits. Since there are a total of $\binom{K}{L}$ combinations of L receive antennas, the RIS-RGSSK utilizes $\lfloor \log_2 \binom{K}{L} \rfloor$ information bits of a transmit symbol to select a combination of the receive antennas. Subsequently, we extend the RIS-RGSSK to the RIS-RGSM, where we use M-ary PSK symbols to convey the additional information bits. Therefore, for the RIS-RGSM, the total number of bits per each transmit IM symbol is given by $\mathcal{B} = \lfloor \log_2 \binom{K}{L} \rfloor + L \log_2(M)$. We denote the ordered set of selected receive-antenna indexes by $\mathcal{S}$ and its lth element by $\mathcal{S}(l)$ for $l = 1, \cdots, L$. Without loss of generality, we assume that $\mathcal{S}(1) < \mathcal{S}(2) < \cdots < \mathcal{S}(L)$, and we denote $\mathcal{C}$ as the code-words set, i.e., the set of all combinations of receive-antenna indexes used at the transmitter. The real part of the signal received at the lth selected antenna is given by

$$y^{\mathcal{R}}_{\mathcal{S}(l)} = \sqrt{E_s} \left(\mathbf{h}^{\mathcal{R}}_{\mathcal{S}(l)} \boldsymbol{\theta}^{\mathcal{R}} - \mathbf{h}^{\mathcal{I}}_{\mathcal{S}(l)} \boldsymbol{\theta}^{\mathcal{I}} \right) + n^{\mathcal{R}}_{\mathcal{S}(l)}. \tag{3.2}$$

Here, $(\cdot)^{\mathcal{R}}$ and $(\cdot)^{\mathcal{I}}$ denote the real and imaginary part, respectively, of a complex scalar/vector.

In the following, we initially present the optimization problem for the proposed RIS-RGSSK scheme. For which, we select the real part of the received signal as our objective function, which means that we use only the in-phase channel for further processing. Its solution is obtained by solving the Karush-Kuhn-Tucker (KKT) conditions. Then, we extend the solution to the RIS-RGSM scheme in Section 3.3.2. We also present non-coherent GDs for both schemes, which have significantly reduced computational complexity than the optimal maximum-likelihood (ML) detectors.

3.3 Problem Formulation and Solution

3.3.1 RIS-RGSSK Scheme

In this scheme, we maximize the minimum of the transmitted signal components in the real part of the received signals at all the selected antennas. Here, unlike [9], we have not

used both real and imaginary components of the received signal in the objective function. This change enables us 1) to select more than two receive antennas, which is not possible in the schemes presented in [9] and 2) to obtain a low-complexity optimal solution that can be applied to the RIS-RGSM.

The RIS-RGSSK optimization problem is formulated as

$$\mathcal{P}1: \max_{\boldsymbol{\theta}^{\mathcal{R}},\boldsymbol{\theta}^{\mathcal{I}}} \min_{l\in\{1,2,\cdots,L\}} \{\mathbf{h}^{\mathcal{R}}_{\mathcal{S}(l)}\boldsymbol{\theta}^{\mathcal{R}} - \mathbf{h}^{\mathcal{I}}_{\mathcal{S}(l)}\boldsymbol{\theta}^{\mathcal{I}}\}, \tag{3.3}$$

$$\text{s.t. } \left(\theta_i^{\mathcal{R}}\right)^2 + \left(\theta_i^{\mathcal{I}}\right)^2 = 1, \quad \forall\ i = 1, 2, \cdots, N. \tag{3.4}$$

The problem $\mathcal{P}1$ is re-expressed using the epigraph form as

$$\mathcal{P}2: \min_{\boldsymbol{\theta}^{\mathcal{R}},\boldsymbol{\theta}^{\mathcal{I}},t} f_0(\boldsymbol{\theta}^{\mathcal{R}},\boldsymbol{\theta}^{\mathcal{I}},t) \triangleq t \tag{3.5}$$

$$\text{s.t. } f_l(\boldsymbol{\theta}^{\mathcal{R}},\boldsymbol{\theta}^{\mathcal{I}},t) \triangleq -\mathbf{h}^{\mathcal{R}}_{\mathcal{S}(l)}\boldsymbol{\theta}^{\mathcal{R}} + \mathbf{h}^{\mathcal{I}}_{\mathcal{S}(l)}\boldsymbol{\theta}^{\mathcal{I}} - t \leq 0, \tag{3.6}$$

$$g_i(\boldsymbol{\theta}^{\mathcal{R}},\boldsymbol{\theta}^{\mathcal{I}},t) \triangleq \left(\theta_i^{\mathcal{R}}\right)^2 + \left(\theta_i^{\mathcal{I}}\right)^2 - 1 = 0, \tag{3.7}$$

for $l = 1, \cdots, L$, and $i = 1, 2, \cdots, N$. Note that the problem $\mathcal{P}2$ is non-convex due to the equality constraints in (3.7). The Lagrange function associated with the problem $\mathcal{P}2$ is given by

$$G(\boldsymbol{\theta}^{\mathcal{R}},\boldsymbol{\theta}^{\mathcal{I}},t,\boldsymbol{\lambda},\boldsymbol{\nu}) = t + \sum_{l=1}^{L}\lambda_l f_l(\boldsymbol{\theta}^{\mathcal{R}},\boldsymbol{\theta}^{\mathcal{I}},t) + \sum_{i=1}^{N}\nu_i g_i(\boldsymbol{\theta}^{\mathcal{R}},\boldsymbol{\theta}^{\mathcal{I}},t), \tag{3.8}$$

where $\boldsymbol{\lambda} = \left[\lambda_1, \cdots, \lambda_L\right]^T \geq 0$ and $\boldsymbol{\nu} = \left[\nu_1, \nu_2, \cdots, \nu_N\right]^T$ are the Lagrange multiplier vectors corresponding to the inequality and equality constraints. Using (3.6) and (3.7), we get

$$\begin{aligned} G(\boldsymbol{\theta}^{\mathcal{R}},\boldsymbol{\theta}^{\mathcal{I}},t,\boldsymbol{\lambda},\boldsymbol{\nu}) = &\left(1 - \sum_{l=1}^{L}\lambda_l\right)t + \sum_{l=1}^{L}\lambda_l\left(-\mathbf{h}^{\mathcal{R}}_{\mathcal{S}(l)}\boldsymbol{\theta}^{\mathcal{R}} + \mathbf{h}^{\mathcal{I}}_{\mathcal{S}(l)}\boldsymbol{\theta}^{\mathcal{I}}\right) \\ &+ \sum_{i=1}^{N}\nu_i\left(\left(\theta_i^{\mathcal{R}}\right)^2 + \left(\theta_i^{\mathcal{I}}\right)^2 - 1\right). \end{aligned} \tag{3.9}$$

The objective function of the dual optimization problem can be obtained from (3.9) as

$$q(\boldsymbol{\lambda},\boldsymbol{\nu}) = \inf_{\boldsymbol{\theta}^{\mathcal{R}},\boldsymbol{\theta}^{\mathcal{I}},t} G(\boldsymbol{\theta}^{\mathcal{R}},\boldsymbol{\theta}^{\mathcal{I}},t,\boldsymbol{\lambda},\boldsymbol{\nu}). \tag{3.10}$$

By setting the gradients of $G(\boldsymbol{\theta}^{\mathcal{R}},\boldsymbol{\theta}^{\mathcal{I}},t,\boldsymbol{\lambda},\boldsymbol{\nu})$ with respect to $\boldsymbol{\theta}^{\mathcal{R}}$, $\boldsymbol{\theta}^{\mathcal{I}}$, and t to zero, we obtain the optimal θ_i's as

$$\tilde{\theta}_i = \frac{\sum_{l=1}^{L}\lambda_l h^*_{\mathcal{S}(l),i}}{2\nu_i}, \quad i = 1, ..., N, \tag{3.11}$$

where $(\cdot)^*$ denotes the conjugation operation and $\sum_{l=1}^{L} \lambda_l = 1$. Note that the Lagrange function in (3.9) is quadratic in $\boldsymbol{\theta}^{\mathcal{R}}$ and $\boldsymbol{\theta}^{\mathcal{I}}$. Therefore, the $q(\boldsymbol{\lambda}, \boldsymbol{\nu})$ would be finite only if $\boldsymbol{\nu} > 0$. Using (3.11) and $\sum_{l=1}^{L} \lambda_l = 1$, $\mathcal{P}2$ can be expressed as

$$\mathcal{P}3 : \min_{\boldsymbol{\lambda}, \boldsymbol{\nu}} -q(\boldsymbol{\lambda}, \boldsymbol{\nu}) \tag{3.12}$$

$$\text{s.t.} \sum_{l=1}^{L} \lambda_l = 1, \tag{3.13}$$

$$\lambda_l \geq 0, \quad \forall\, l = 1, \cdots, L, \tag{3.14}$$

$$\nu_i > 0, \quad \forall\, i = 1, 2, \cdots, N, \tag{3.15}$$

where

$$q(\boldsymbol{\lambda}, \boldsymbol{\nu}) = -\sum_{i=1}^{N} \left(\frac{1}{4\nu_i} \left| \sum_{l=1}^{L} \lambda_l h_{\mathcal{S}(l),i} \right|^2 + \nu_i \right). \tag{3.16}$$

By equating the gradient of $q(\boldsymbol{\lambda}, \boldsymbol{\nu})$ with respect to $\boldsymbol{\nu}$ to zero and using the positive solution, we get

$$\tilde{\nu}_i = \frac{1}{2} \left| \sum_{l=1}^{L} \lambda_l h_{\mathcal{S}(l),i} \right|. \tag{3.17}$$

By using (3.17), the problem $\mathcal{P}3$ simplifies to

$$\mathcal{P}4 : \min_{\boldsymbol{\lambda}} \sum_{i=1}^{N} \left| \sum_{l=1}^{L} \lambda_l h_{\mathcal{S}(l),i} \right| \tag{3.18}$$
$$\text{s.t. (3.13) and (3.14).}$$

The equality constraint in the above optimization problem can be removed by substituting $\lambda_L = 1 - \sum_{l=1}^{L-1} \lambda_l$ in the objective function. The updated optimization problem becomes

$$\mathcal{P}5 : \min_{\boldsymbol{\lambda}} \sum_{i=1}^{N} \left| h_{\mathcal{S}(L),i} + \sum_{l=1}^{L-1} \lambda_l \left(h_{\mathcal{S}(l),i} - h_{\mathcal{S}(L),i} \right) \right| \tag{3.19}$$

$$\text{s.t.} \sum_{l=1}^{L-1} \lambda_l \leq 1, \tag{3.20}$$

$$\lambda_l \geq 0, \quad \forall\, l = 1, \cdots, L-1. \tag{3.21}$$

For this problem $\mathcal{P}5$, the associated Lagrange function is

$$G^{(1)}(\boldsymbol{\lambda}, \boldsymbol{\alpha}, \beta) = \sum_{i=1}^{N} |A_i(\boldsymbol{\lambda})| - \sum_{l=1}^{L-1} \alpha_l \lambda_l + \beta \left(\sum_{l=1}^{L-1} \lambda_l - 1 \right), \tag{3.22}$$

where $\beta \geq 0$ and $\alpha_l \geq 0$ are the Lagrange multipliers, and

$$A_i(\boldsymbol{\lambda}) = h_{S(L),i} + \sum_{j=1}^{L-1} \lambda_j \left(h_{S(j),i} - h_{S(L),i} \right). \tag{3.23}$$

Since $\mathcal{P}5$ is a convex problem, any points satisfying the KKT conditions are primal and dual optimal. Thus, for the problem (3.22), the KKT conditions, $\forall\ l = 1, \cdots, L-1$, are stated as: $\tilde{\lambda}_l \geq 0$, $\sum_{l=1}^{L-1} \tilde{\lambda}_l - 1 \leq 0$, $\tilde{\alpha}_l \geq 0$, $\tilde{\beta} \geq 0$, $\tilde{\alpha}_l \tilde{\lambda}_l = 0$,

$$\tilde{\beta} \left(\sum_{l=1}^{L-1} \tilde{\lambda}_l - 1 \right) = 0, \tag{3.24}$$

$$\sum_{i=1}^{N} \frac{\left(\left(h_{S(l),i} - h_{S(L),i} \right)^* A_i(\tilde{\boldsymbol{\lambda}}) \right)^{\mathcal{R}}}{\left| A_i(\tilde{\boldsymbol{\lambda}}) \right|} - \tilde{\alpha}_l + \tilde{\beta} = 0. \tag{3.25}$$

From the KKT conditions, we have a total of 2^L cases corresponding to whether $\tilde{\lambda}_l = 0$ or $\tilde{\lambda}_l > 0$ for $l = 1, \cdots, L-1$ and $1 - \sum_{j=1}^{L-1} \tilde{\lambda}_j = \tilde{\lambda}_L = 0$, or $\tilde{\lambda}_L > 0$. Among all the cases, $\tilde{\lambda}_l = 0$ for $l = 1, 2, \cdots, L$ is infeasible, as $\tilde{\lambda}_L = 1 - \sum_{j=1}^{L-1} \tilde{\lambda}_j$. As such, at least one of $\tilde{\lambda}_l$'s, $l = 1, 2, \cdots, L$, must be positive. Without loss of generality, we assume that, $\tilde{\lambda}_L = 1 - \sum_{j=1}^{L-1} \tilde{\lambda}_j > 0$. Consequently, (3.24) implies that $\tilde{\beta} = 0$. Therefore, (3.25) simplifies to

$$f\left(\tilde{\boldsymbol{\lambda}}, l \right) \triangleq \sum_{i=1}^{N} \frac{\left(\left(h_{S(l),i} - h_{S(L),i} \right)^* A_i(\tilde{\boldsymbol{\lambda}}) \right)^{\mathcal{R}}}{\left| A_i(\tilde{\boldsymbol{\lambda}}) \right|} = \tilde{\alpha}_l. \tag{3.26}$$

From the KKT conditions, we can have the following two cases for each l: $\tilde{\alpha}_l > 0$ and $\tilde{\lambda}_l = 0$; and $\tilde{\alpha}_l = 0$. For the first case, $A_i(\boldsymbol{\lambda})$, as defined in (3.23), becomes independent of $h_{\mathcal{S}(l),i}$ because of $\tilde{\lambda}_l = 0$. Using the central-limit theorem, it can be shown that it is extremely unlikely that $f(\boldsymbol{\lambda}, l)$, as defined in (3.26), becomes positive. As such, the first case is extremely unlikely to occur. In other words, the second case, i.e., $\tilde{\alpha}_l = 0$, will occur with very high probability, and (3.25) simplifies to

$$f\left(\tilde{\boldsymbol{\lambda}}, l \right) = \sum_{i=1}^{N} \frac{\left(\left(h_{S(l),i} - h_{S(L),i} \right)^* A_i(\tilde{\boldsymbol{\lambda}}) \right)^{\mathcal{R}}}{\left| A_i(\tilde{\boldsymbol{\lambda}}) \right|} = 0, \tag{3.27}$$

for $l = 1, \cdots, L-1$. Consequently, solving the optimization problem (3.3) reduces to solving a system of L equations formed by $\sum_{l=1}^{L} \lambda_l = 1$ and (3.27), then $\{\tilde{\nu}_i\}$ is obtained via (3.17), and the reflection coefficients $\left\{\tilde{\theta}_i\right\}$ are obtained by substituting (3.17) in (3.11), which is expressed as follows

$$\tilde{\theta}_i = \frac{\sum_{l=1}^{L} \tilde{\lambda}_l h^*_{\mathcal{S}(l),i}}{\left|\sum_{l=1}^{L} \tilde{\lambda}_l h_{\mathcal{S}(l),i}\right|}, \forall\ i = 1, 2, \cdots, N. \tag{3.28}$$

RIS-RGSSK Reception: The ML detector of the RIS-RGSSK scheme is given by

$$\hat{\mathcal{S}}_{\mathrm{ML}} = \arg\min_{\mathcal{S}} \sum_{k=1}^{K} \left| y_k - \sqrt{E_s}\mathbf{h}_k \widetilde{\boldsymbol{\theta}}\left(\mathcal{S}\right)\right|^2, \tag{3.29}$$

where $\widetilde{\boldsymbol{\theta}}\left(\mathcal{S}\right)$ is the vector of optimal phase shifts of the RIS elements corresponding to the selected antennas $\mathcal{S}$ as given by (3.28). Observe that the ML receiver requires the complete channel state information (CSI) at the receiver. Moreover, it is computationally intensive. To address these issues with the optimal ML receiver, we present the following low-complexity GD.

The proposed GD determines the selected receive antennas without requiring CSI. First, the detector estimates $L-1$ indexes as $\hat{\mathcal{S}}_1 = \arg\max_{\text{L-1}1 \le l \le K} \left\{y_l^{\mathcal{R}}\right\}$, where $\arg\max_{\text{L-1}}\{\cdot\}$ returns the set of $L-1$ maximum values. The estimated set $\hat{\mathcal{S}}_1$ is then used to find the range of the last index using the final-index range finder proposed in [11]. We denote the range of the last index by r, which guarantees that the estimated index set, $\hat{\mathcal{S}}$, lies in the code book used at the transmitter, $\mathcal{C}$. Then, the last index is estimated as $\hat{l}_F = \arg\max_{l \in r} \left\{y_l^{\mathcal{R}}\right\}$. Finally, $\hat{\mathcal{S}}$ is obtained by sorting the elements of $\hat{\mathcal{S}}_1 \cup \{\hat{l}_F\}$.

3.3.2 RIS-RGSM Scheme

In the following, we first explain the proposed RIS-RGSM scheme for single receive antenna selection, and then we extend it to the selection of more than one receive antenna. For single receive antenna selection (i.e., when $L = 1$), the proposed RIS-RGSSK scheme optimizes $\boldsymbol{\theta}$ as $\tilde{\theta}_i = h^*_{\mathcal{S}(1),i}/|h_{\mathcal{S}(1),i}|$, for $i = 1, 2, \cdots, N$ as $\sum_{l=1}^{L} \lambda_l = 1$ simplifies to $\lambda_1 = 1$. In order to convey additional information using a PSK-modulated symbol, we modify $\tilde{\theta}_i$ as

$$\tilde{\theta}_i = x_1 \frac{h^*_{\mathcal{S}(1),i}}{|h_{\mathcal{S}(1),i}|} = \frac{\left(x_1^* h_{\mathcal{S}(1),i}\right)^*}{|x_1^* h_{\mathcal{S}(1),i}|}, \tag{3.30}$$

where x_1 is the PSK-modulated symbol with unit power, i.e., $|x_1| = 1$. The modification, as given by (3.30), ensures that the received signal at the selected antenna depends on the phase of the PSK-modulated symbol x_1. From (3.30), $\boldsymbol{\theta}$ can also be obtained by solving the following optimization problem

$$\tilde{\boldsymbol{\theta}} = \underset{\left(\theta_i^{\mathcal{R}}\right)^2+\left(\theta_i^{\mathcal{I}}\right)^2=1}{\arg\max} \left(x_1^* \mathbf{h}_{\mathcal{S}(1)}\right)^{\mathcal{R}} \boldsymbol{\theta}^{\mathcal{R}} - \left(x_1^* \mathbf{h}_{\mathcal{S}(1)}\right)^{\mathcal{I}} \boldsymbol{\theta}^{\mathcal{I}}. \tag{3.31}$$

Note that if the absolute value had been used instead of the real part of $x_1^* \mathbf{h}_{\mathcal{S}(1)} \boldsymbol{\theta}$, the solution would not have been unique. As a result, the objective function maximizing the objective function would not ensure that the received signal at the selected receive antenna depends on the phase of the PSK-modulated symbol x_1. That explains why we choose the real part instead of the absolute value of the transmitted signal component as the objective function in the optimization problems for both RIS-RGSSK and RIS-RGSM schemes.

For the selection of more than one receive antenna, the proposed RIS-RGSM scheme generalizes the optimization problem given in (3.31) as follows

$$\mathcal{P}6: \max_{\boldsymbol{\theta}^{\mathcal{R}}, \boldsymbol{\theta}^{\mathcal{R}}} \min_{l \in \{1,2,\cdots,L\}} \left\{ \left(x_l^* \mathbf{h}_{\mathcal{S}(l)}\right)^{\mathcal{R}} \boldsymbol{\theta}^{\mathcal{R}} - \left(x_l^* \mathbf{h}_{\mathcal{S}(l)}\right)^{\mathcal{I}} \boldsymbol{\theta}^{\mathcal{I}} \right\}, \tag{3.32}$$

$$\text{s.t. } \left(\theta_i^{\mathcal{R}}\right)^2 + \left(\theta_i^{\mathcal{I}}\right)^2 = 1, \quad \forall\ i = 1, 2, \cdots, N. \tag{3.33}$$

The problem $\mathcal{P}6$ is closely related to the problem $\mathcal{P}1$, with the only difference that $\mathbf{h}_{\mathcal{S}(l)}$ is replaced by $x_l^* \mathbf{h}_{\mathcal{S}(l)}$. Hence, similar to the proposed RIS-RGSSK scheme, $\tilde{\boldsymbol{\theta}}$ for the proposed RIS-RGSM scheme is obtained as

$$\tilde{\theta}_i = \frac{\sum_{l=1}^{L} \tilde{\lambda}_l x_l h_{\mathcal{S}(l),i}^*}{\left| \sum_{l=1}^{L} \tilde{\lambda}_l x_l^* h_{\mathcal{S}(l),i} \right|}, \quad \forall\ i = 1, 2, \cdots, N, \tag{3.34}$$

where $\tilde{\lambda}_l$ for $l = 1, 2, \cdots, L$ are obtained using $\tilde{\lambda}_L = 1 - \sum_{j=1}^{L-1} \tilde{\lambda}_j$, and solving the following $L - 1$ equations simultaneously.

$$\sum_{i=1}^{N} \frac{\left(\left(x_l^* h_{S(l),i} - x_L^* h_{S(L),i}\right)^* B_i(\tilde{\boldsymbol{\lambda}}) \right)^{\mathcal{R}}}{\left| B_i(\tilde{\boldsymbol{\lambda}}) \right|} = 0, \tag{3.35}$$

for

$$B_i(\tilde{\boldsymbol{\lambda}}) = x_L^* h_{S(L),i} + \sum_{j=1}^{L-1} \tilde{\lambda}_j \left(x_j^* h_{S(j),i} - x_L^* h_{S(L),i} \right). \tag{3.36}$$

RIS-RGSM Reception: Similar to the RIS-RGSSK scheme, the optimal ML detector can be shown to be

$$\left(\hat{\mathcal{S}}_{\mathrm{ML}}, \hat{x}_{\mathrm{ML}}\right) = \arg\min_{\mathcal{S},x} \sum_{k=1}^{K} \left| y_k - \sqrt{E_s}\mathbf{h}_k \widetilde{\boldsymbol{\theta}}\left(\mathcal{S}, x\right) \right|^2, \tag{3.37}$$

where $\widetilde{\boldsymbol{\theta}}\left(\mathcal{S}, x\right)$ is the vector of optimum phase shifts of the RIS elements corresponding to both the selected antennas $\mathcal{S}$ and the extra information bits x. Since the optimal receiver requires the complete CSI and is highly computationally intensive, we present the following GD.

For the proposed GD, the receiver first detects the selected receive antenna indexes without requiring any CSI and then retrieves the extra information bits $\hat{x}_l$ from the phase of the received signal at estimated receive antenna indexes. Similar to the RIS-RGSSK scheme, the RIS-RGSM receiver estimates the receive antenna indexes by first finding the $L-1$ indexes $\hat{\mathcal{S}}_1 = \arg\max_{\text{L-1}1 \le l \le K} |y_l|$ and then estimating the last index $\hat{l}_F = \arg\max_{l \in r} |y_l|$. The estimated set $\hat{\mathcal{S}}$ is obtained by sorting the elements of $\hat{\mathcal{S}}_1 \cup \{\hat{l}_F\}$. After estimating the selected indexes, the transmitted M-PSK symbols are estimated non-coherently as

$$\hat{x}_l = \arg\max_{x_l \in \mathcal{X}} \left\{ (y_{\hat{\mathcal{S}}(l)} x_l^*)^{\mathcal{R}} \right\}, \quad \forall\, l = 1, \cdots, L, \tag{3.38}$$

where $\arg\max\{\cdot\}$ returns the maximum value of its argument, and $\mathcal{X}$ is the M-PSK modulating set used at the transmitter.

3.3.3 Complexity Analysis

In the following, we provide the computational complexities of the proposed greedy and the optimal ML detectors.

For the RIS-RGSM, the computational complexity of the proposed GD is as follows: The detection of the L maximum values out of K values of the real part of the received signal has a complexity of $O(K \log L)$. Also, retrieving the extra information bits through (3.38) is of $O(LM)$. As such, the complexity of the GD for RIS-RGSM scheme is given by $O(K \log L + LM)$. For the RIS-RGSSK scheme, the computational complexity is just $O(K \log L)$.

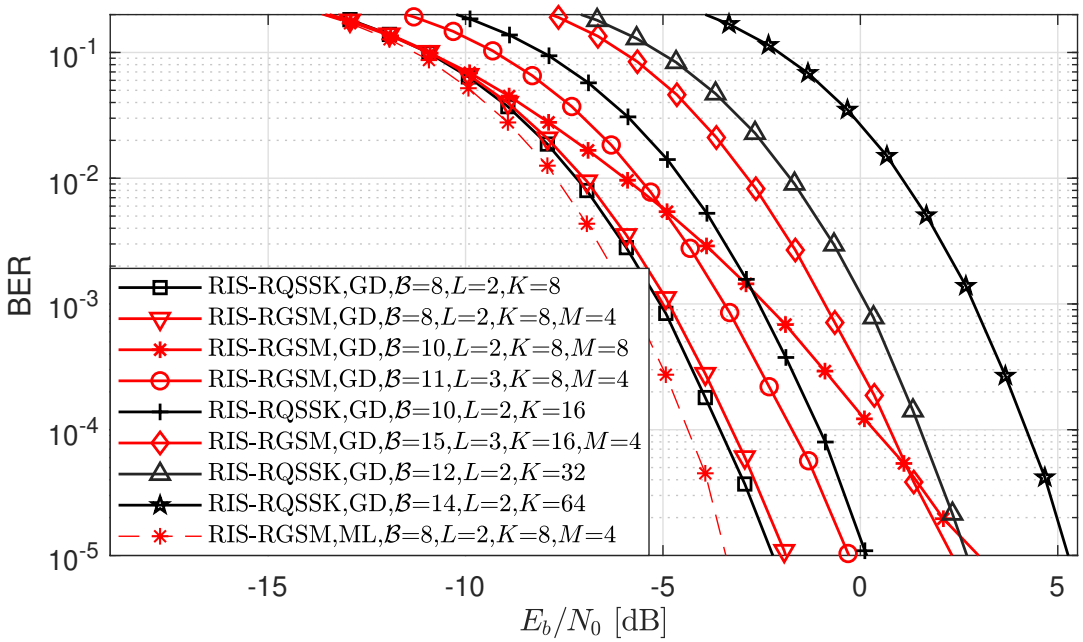

Figure 3.2: Comparison of the proposed RIS-RGSM (with $K = 8$, and 16) and the RIS-RQSSK (with $K = 8$, 16, 32, and 64) schemes for $L = 2$, and 3, at $N = 128$.

For the optimal ML detector in (3.37), the optimal phase calculation as given by (3.34) requires solving a set of L equations to determine optimal λ's, whose complexity is $O(L^3)$. Given optimal λ's, the complexity of (3.34) is $O(NL)$. Since the optimal phase values are computed $M\binom{K}{L}$ times, the complexity of the optimal phase calculation is $O\left(M(L^3 + NL)K^L\right)$. Furthermore, (3.37) requires evaluation of K dot products of vectors of size N for each of $M\binom{K}{L}$ combinations. As such, the complexity of implementing (3.37) given the optimal phase values is $O\left(NMK^{L+1}\right)$. Using the afore-mentioned complexities, the computational complexity of the optimal ML detector can be shown to be $O\left(M(L^3 + KN) \cdot K^L\right)$. For the RIS-RGSKK scheme, the complexity can similarly be shown to be $O\left((L^3 + KN) \cdot K^L\right)$.

Observe that the proposed GDs have significantly less computational complexity than the ML detectors.

3.4 Simulation Results

In this section, we present simulation results to evaluate the performance of the proposed RIS-RGSSK and RIS-RGSM schemes. Here, we define the SNR in dB to be equal to E_s/N_0,

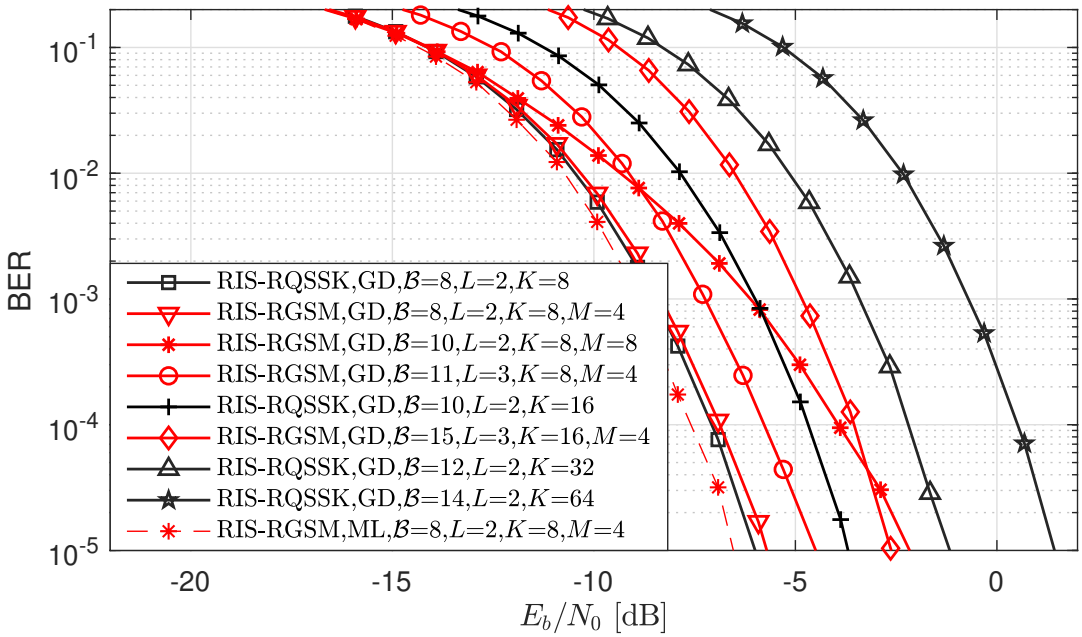

Figure 3.3: Comparison of the proposed RIS-RGSM (with $K = 8$, and 16) and the RIS-RQSSK (with $K = 8$, 16, 32, and 64) schemes for $L = 2$, and 3, at $N = 256$.

and the relation between E_s/N_0 and E_b/N_0 is given as $E_b/N_0 = E_s/N_0 + 10\log_{10}(N \times K) - 10\log_{10}(\mathcal{B})$. Following [9], a key point to observe is the consistent relationship between the elements of optimal $\tilde{\boldsymbol{\lambda}}$. Taking into consideration that all $h^{\mathcal{R}}_{S(l),i}$, $h^{\mathcal{I}}_{S(l),i}$, $l = 1, ..., L$ and $i = 1, 2, ..., N$, are RVs identically distributed as $\mathcal{N}\left(0, \frac{1}{2}\right)$, this implies that $\tilde{\lambda}_l$, $\forall\, l = 1, \cdots, L$, as calculated from (3.27) or (3.35) have equal mean[1], i.e., $\mathbb{E}\{\tilde{\lambda}_l\} = 1/L$, $l = 1, ..., L$.

Fig. 3.2 illustrates the BER of our proposed RIS-RGSM scheme compared to the RIS-RQSSK scheme (with polarity bits) from [9], with $N = 128$. Various configurations are presented for the RIS-RGSM scheme to achieve $\mathcal{B} = 8$, 10, 11, and 15. For the RIS-RQSSK with $K = 8$, 6 bits are conveyed through index selection, and an additional 1 bit is transmitted per selected antenna, resulting in a total $\mathcal{B} = 6 + 2 = 8$ bits per symbol. In the case where both schemes operate with $\mathcal{B} = 8$, the proposed RIS-RGSM demonstrates competitive performance, trailing RIS-RQSSK by only 0.3 dB at a BER of 10^{-5}. Furthermore,

[1]Based on the recommendations of the Advisory Committee, the histogram of the parameter $\tilde{\lambda}_1$ and the impact of the approximation of $\boldsymbol{\lambda}$ on the BER of the proposed RIS-RGSSK scheme are presented in Appendix A.

increasing M beyond 4, e.g., using 8-PSK while selecting $L = 2$ out of $K = 8$ antennas, results in a degradation of BER performance at higher E_b/N_0. Upon increasing $\mathcal{B}$ to 11 for the RIS-RGSM scheme ($L = 3$ out of $K = 8$ using QPSK) and the RIS-RQSSK achieving $\mathcal{B} = 10$ (with $K = 16$ and $L = 2$), our proposed RIS-RGSM outperforms the RIS-RQSSK by 0.6 dB, transmitting 10% more bits. Additionally, at $\mathcal{B} = 15$ ($L = 3$ out of $K = 16$ using QPSK), the proposed RIS-RGSM exhibits a noteworthy 3.0 dB improvement in BER compared to the RIS-RQSSK at $\mathcal{B} = 14$ ($K = 64$ and $L = 2$).

In Fig. 3.3, we depict the BER performance for the parameters used in Fig. 3.2 but for $N = 256$. The results show that when $\mathcal{B} = 8$, the BER performance advantage of the RIS-RQSSK becomes less significant compared to our RIS-RGSM as N increases from 128 to 256, presenting a margin of only 0.2 dB for the same BER of 10^{-5}. Overall, the results show that for higher $\mathcal{B}$ and larger N, our proposed RIS-RGSM can evidently outperforms the RIS-RQSSK, e.g., 4.0 dB improvement in E_b/N_0 of the proposed RIS-RGSM ($\mathcal{B} = 15$) compared to the RIS-RQSSK ($\mathcal{B} = 14$). One can also see from Fig. 3.2 and Fig. 3.3 that the proposed non-coherent GD approaches the ML performance for the same system parameters.

3.5 Conclusion

In this paper, we explored two innovative schemes, RIS-RGSSK and RIS-RGSM. We introduced these schemes, allowing the selection of multiple receive antennas instead of being limited to one or two. We formulated and solved an optimization problem for RIS-RGSSK, maximizing the real component of the received signal. The proposed RIS-RGSM scheme extends the RIS-RGSSK scheme by embedding extra information in the phase of the transmitted signal using M-PSK modulation by solving an extended optimization problem. Our simulation results showed that, as the number of the RIS reflecting elements increases, the proposed RIS-RGSM can achieve both a better BER performance and a higher bit rate compared to the recent RIS-RQSSK benchmark, e.g., 4.0 dB improvement in E_b/N_0 when $N = 256$.

Appendix

We provide the histogram of the optimum $\tilde{\lambda}_1$ in Fig. 3.4 for the case of $L = 3$. We considered 10^5 channel realizations, and for each realization, we solved the system of L equations formed by $\sum_{l=1}^{L} \lambda_l = 1$ and (3.27) numerically to obtain the optimal values of $\tilde{\lambda}_1, \tilde{\lambda}_2$, and $\tilde{\lambda}_3$. It is observed that $\tilde{\lambda}_1, \tilde{\lambda}_2$ and $\tilde{\lambda}_3$ closely follows a Gaussian distribution with mean $\frac{1}{L} = \frac{1}{3}$, i.e., $\tilde{\lambda}_l \sim \mathcal{N}\left(\frac{1}{L}, \sigma^2_{\tilde{\lambda}_l}\right)$, $l = 1, ..., L$, and that the variance $\sigma^2_{\tilde{\lambda}_l}$ decreases with increasing N. Since the impact of an optimal value of $\tilde{\lambda}_l$ diminishes as N increases, we can use an approximated value of $\tilde{\lambda}_l = 1/L$ especially for very large values of N.

Fig. 3.5 shows the effect of the optimal value of $\tilde{\boldsymbol{\lambda}}$ versus its approximated value, we plot the BER of the proposed RIS-RGSSK as a function of the E_b/N_0 for $N = 64$, 128, and 256, $K = 8$, $L = 3$, and optimal and approximated values of $\boldsymbol{\lambda}$. Since we have $L = 3$, we approximate the values of $\lambda_1 = \lambda_2 = \lambda_3 = \frac{1}{3}$. As can be seen from Fig. 3.5, the BER performance with approximated $\boldsymbol{\lambda}$ approach its counterparts of optimal $\tilde{\boldsymbol{\lambda}}$ at $N = 128$ and 256. While at $N = 64$, one can observe a degradation in the BER performance. Such results align with Fig. 3.4, where the standard deviation for $N = 64$ is observed to be larger than for $N = 128$ and 256.

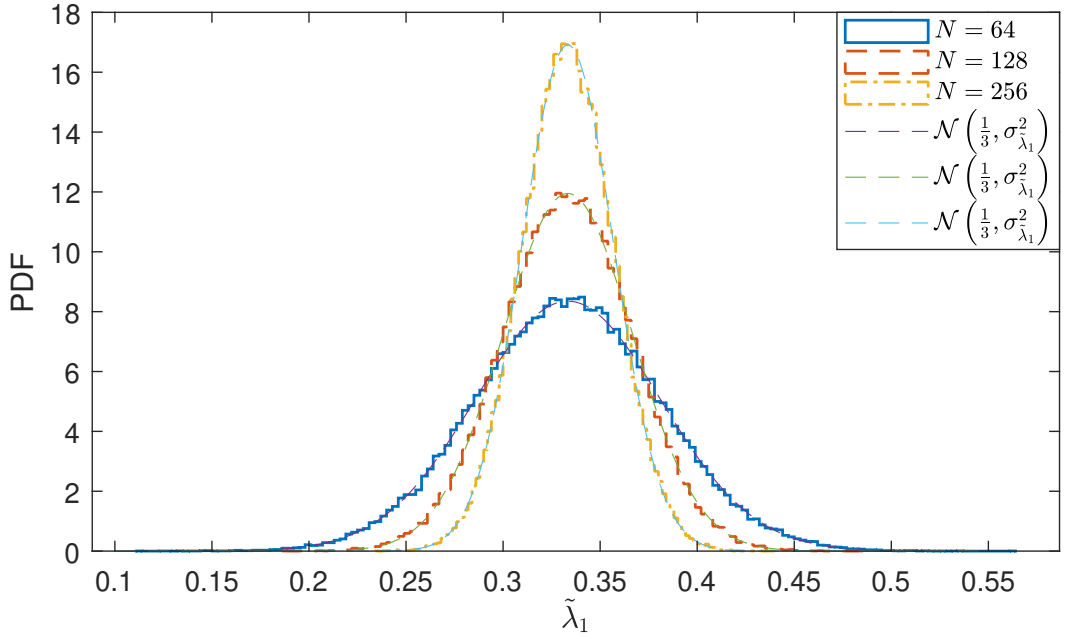

Figure 3.4: Histogram of the parameter $\tilde{\lambda}_1$.

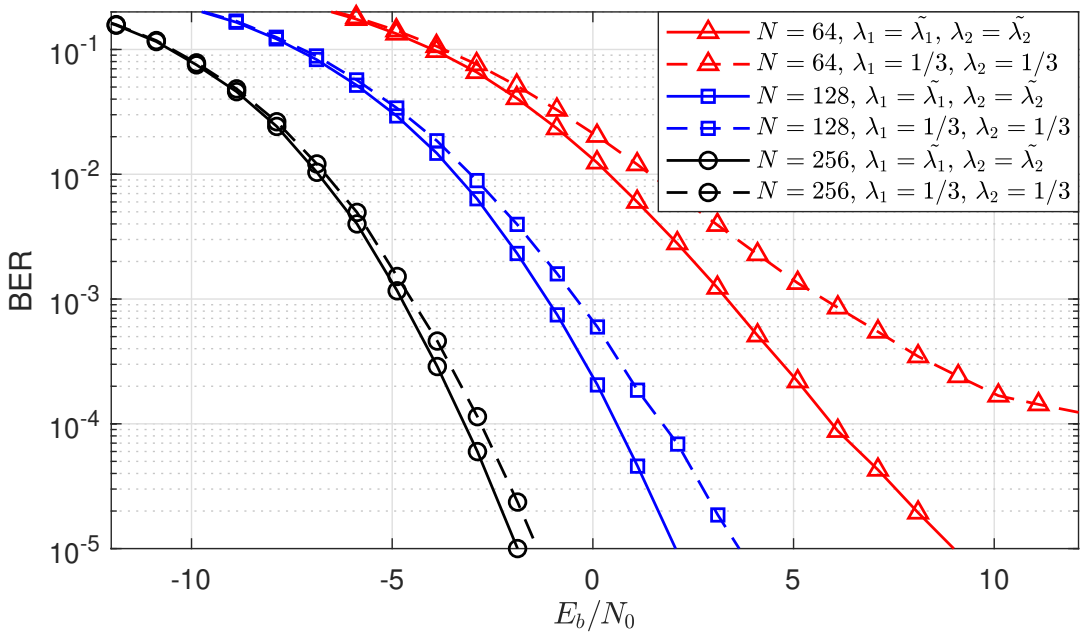

Figure 3.5: Impact of the approximation of $\boldsymbol{\lambda}$ on the BER of the proposed RIS-RGSSK scheme at $N = 64$, 128, and 256, for $K = 8$, $L = 3$, and $\mathcal{B} = 5$.

References

[1] E. Basar, M. Di Renzo, J. De Rosny, M. Debbah, M.-S. Alouini, and R. Zhang, "Wireless communications through reconfigurable intelligent surfaces," *IEEE Access*, vol. 7, pp. 116 753–116 773, 2019.

[2] X. Zhu, W. Chen, Q. Wu, Z. Li, J. Li, S. Zhang, and M. Ding, "Reconfigurable intelligent surface aided space shift keying with imperfect CSI," *IEEE Internet Things J.*, Nov. 2023.

[3] X. Zhu, L. Yuan, Q. Li, L. Jin, X. Nie, C. Pan, and J. Zhang, "RIS-assisted full-duplex space shift keying: System scheme and performance analysis," *IEEE Trans. Green Commun. Netw.*, Jul. 2023.

[4] J. Li, S. Dang, M. Wen, Q. Li, Y. Chen, Y. Huang, and W. Shang, "Index modulation multiple access for 6G communications: Principles, applications, and challenges," *IEEE Netw.*, vol. 37, no. 1, pp. 52–60, Jan./Feb. 2023.

[5] A. E. Canbilen, E. Basar, and S. S. Ikki, "Reconfigurable intelligent surface-assisted space shift keying," *IEEE Wireless Commun. Lett.*, vol. 9, no. 9, pp. 1495–1499, Jan. 2020.

[6] W. Yan, X. Yuan, Z.-Q. He, and X. Kuai, "Passive beamforming and information transfer design for reconfigurable intelligent surfaces aided multiuser MIMO systems," *IEEE J. Sel. Areas Commun.*, vol. 38, no. 8, pp. 1793–1808, Aug. 2020.

[7] S. Lin, B. Zheng, G. C. Alexandropoulos, M. Wen, M. Di Renzo, and F. Chen, "Reconfigurable intelligent surfaces with reflection pattern modulation: Beamforming design and performance analysis," *IEEE Trans. Wireless Commun.*, vol. 20, no. 2, pp. 741–754, Feb. 2021.

[8] E. Basar, "Reconfigurable intelligent surface-based index modulation: A new beyond

MIMO paradigm for 6G," *IEEE Trans. Commun.*, vol. 68, no. 5, pp. 3187–3196, May 2020.

[9] M. H. Dinan, N. S. Perović, and M. F. Flanagan, "RIS-assisted receive quadrature space-shift keying: A new paradigm and performance analysis," *IEEE Trans. Commun.*, vol. 70, no. 3, pp. 6874–6889, Oct. 2022.

[10] M. H. Dinan, M. Di Renzo, and M. F. Flanagan, "RIS-assisted receive quadrature spatial modulation with low-complexity greedy detection," *IEEE Trans. Commun.*, vol. 71, no. 11, pp. 6541–6560, Nov. 2023.

[11] M. Hanif and H. H. Nguyen, "Frequency-shift chirp spread spectrum communications with index modulation," *IEEE Internet Things J.*, vol. 8, no. 24, pp. 17 611–17 621, Dec. 2021.

4. Performance Analysis of RIS-Assisted Receive Generalized Space Shift Keying and Generalized Spatial Modulation

Submitted as:

P. A. Marín, M. Hanif, and E. Bedeer, "Performance analysis of RIS-assisted receive generalized space shift keying and generalized spatial modulation," under review.

This chapter contains the manuscript of the paper which has been submitted for publication. In this paper, we analyze the performance of both the reconfigurable intelligent surfaces (RIS)-assisted receive generalized space-shift keying (RGSSK) and RIS-assisted receive generalized spatial modulation (RIS-RGSM) developed in the previous chapter. We derive closed-form expressions for the pairwise error probabilities (PEPs) of both RIS-RGSSK and RIS-RGSM schemes when two antennas are activated at the receiver. Our analytical results are validated through simulations.

Performance analysis of RIS-assisted receive generalized space shift keying and generalized spatial modulation

Porfirio A. Marín, Muhammad Hanif, and Ebrahim Bedeer

Abstract

This paper analyzes the performance of the reconfigurable intelligent surfaces (RIS)-assisted receive generalized space-shift keying (RGSSK) and the RIS-assisted receive generalized spatial modulation (RIS-RGSM). Specifically, we find closed-form expressions of the pairwise error probabilities (PEPs) of the RIS-RGSSK and the RIS-RGSM schemes when two antennas are activated at the receiver. Finally, we verify our analytical results via simulations.

Keywords

Greedy detector, multiple antenna selection, pairwise error probabilities (PEPs), performance analysis, RIS-assisted communication.

4.1 Introduction

The 5th generation (5G) wireless communications have marked the beginning of a new era of communication systems, increasing the number of users, services, and use cases. Such growth underscores the need for new and improved technologies to meet future traffic demands. To address these demands, researchers have focused on modifications at the physical layer, developing strategies to control the propagation channel, such as reconfigurable intelligent surfaces (RISs). RIS is considered a potential key for defining the future wireless communications and beyond [1].

RIS has the potential to control signal propagation, leading to significant spectral efficiency (SE) improvements in wireless communications [2]. A widely adopted model of RIS consists of a two-dimensional, extensive, and slender metasurface, made of metallic or dielectric materials, and equipped with an array of passive aperiodic or periodic sub-wavelength electric or magnetic resonators [1]. Its elements can be controlled in a software-defined man-

ner to modify the electromagnetic (EM) properties related to the reflection of incident radio frequency (RF) signals [1]. Ultra-thin design, low signal loss, and simple fabrication make two-dimensional RIS a compelling candidate for communication applications. Hence, RIS is expected to play a key role in future wireless communications systems [2].

Furthermore, index modulation (IM) has become popular due to its ability to increase bits per channel usage by adding extra spatial symbols. IM is a modulation technique that transmits information bits through the activation states in various domains such as space, time, and frequency. IM works by separating information bits into index bits, which specify active resources such as antennas or sub-carriers, and constellation bits, which map symbols into these activated resources. Thus, IM improves SE by utilizing additional index domains to carry more information and enhances energy efficiency (EE) by activating only the necessary transmission entities, reducing power consumption. Consequently, integrating IM into RIS-assisted systems will enhance their performance [1].

In the exploration of IM within RIS-assisted systems, the authors in [3] proposed the RIS-assisted space shift keying (RIS-SSK), which performs IM using a single receive antenna. Here, analytical derivations are provided through the integration of moment-generating function expressions, and upper bounds of the error probability are presented. In [4], the authors proposed utilizing the spatial modulation (SM) principle in a RIS-based system to transmit additional information bits. In which, the performance analysis of the system provides some approximations of the outage probability. The authors in [5] introduced two schemes: RIS-based receive antenna space-shift keying (RIS-RSSK) and RIS-based receive spatial modulation (RIS-RSM). Both schemes utilize IM for a single selected receive antenna, and their performance analysis yields an upper-bounded pairwise error probability (PEP). In [5], the PEPs are calculated via infinite integration of characteristic functions utilizing Gil-Pelaez's inversion formula, which may introduce complexities for practical evaluation. Furthermore, the study in [6] elaborates on these principles with the RIS-assisted receive quadrature space-shift keying (RIS-RQSSK), which derives PEP expressions based on its greedy detector (GD). The GD implemented in [6] detects the antenna indexes by maximizing the squared real or imaginary part of the received signal, and this method is used to derive approximations for

the PEP, including Chernoff bounds and Pearson approximations. However, despite these approximations, the RIS-RQSSK scheme in [6] remains fundamentally limited by its inability to support multiple receive antenna selection. The authors in [7] presented two schemes: the RIS-assisted receive generalized space-shift keying (RIS-RGSSK) and the RIS-assisted receive generalized spatial modulation (RIS-RGSM), where the first one operates based on the principle of generalized space-shift keying (GSSK) for the multiple received antenna activation, and in the RIS-RGSM not only information bits are conveyed through the indexes of selected multiple receive antennas, but additional information bits are also conveyed via the received signal phase (i.e., using M-ary phase shift keying (PSK) modulation) at each selected antenna. In [7], the system performance of both RIS-RGSSK and RIS-RGSM schemes are presented via simulations; however, there is not theoretical analysis of their performance that validates the observed results.

This paper analyzes the performance of the RIS-RGSSK and RIS-RGSM schemes described in [7]. We find closed-form expressions of the PEPs of both schemes, eliminating the need for approximations, numerical methods, or integration processes to pursue the results. For our analysis and to make the derivations tractable, we consider that two antennas are activated at the receiver. These derivations focused on the GD of each scheme. Our approach includes presenting closed-form expressions for the PEPs of both schemes. Finally, we verify our theoretical PEP results with simulations.

The remainder of the paper is structured as follows. Section II presents the RIS-RGSSK and RIS-RGSM schemes. In Section III, we derive the PEPs of both schemes. Then, comparisons between theoretical and simulation-based results of the performance of both schemes are provided in Section IV. Finally, Section V concludes this paper.

4.2 System Model

We adopt the system model in [7], where the RIS-RGSSK and RIS-RGSM schemes utilize the RIS as an access point to convey information through its N reflecting elements to a receiver equipped with K antennas. These RIS elements reflect incident waves from a nearby RF source, with their phases controlled by an RIS controller, which receives information bits

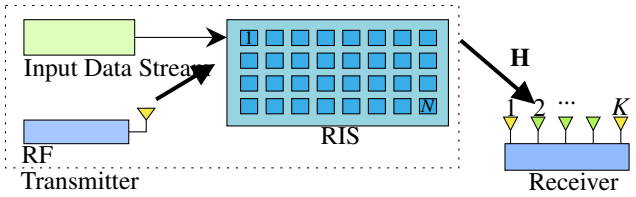

Figure 4.1: A schematic of the proposed RIS-RGSSK system.

as input as illustrated in Fig. 4.1. The baseband complex channel gains linking the RIS elements to the kth receive antenna are symbolized as $\mathbf{h}_k = \begin{bmatrix} h_{k,1}, & h_{k,2}, & \cdots, & h_{k,N} \end{bmatrix}$, where $k = 1, 2, \cdots, K$. Consequently, the baseband received signal at the kth receive antenna is formulated as:

$$y_k = \sqrt{E_s}\mathbf{h}_k\boldsymbol{\theta} + n_k, \tag{4.1}$$

where E_s represents the energy of RF waves reflected by each RIS element per IM symbol. The term n_k stands for zero-mean additive white Gaussian noise at the kth receive antenna, characterized by a variance of σ^2. Additionally, $\boldsymbol{\theta}$ is an N-dimensional complex column vector. Each element θ_i in $\boldsymbol{\theta}$ represents the reflection coefficient of the ith reflecting element, where $|\theta_i| = 1$ for $i = 1, 2, \ldots, N$. Here, we assume lossless reflection from the RIS.

This system consists of two modulation techniques: RIS-RGSSK and RIS-RGSM schemes. A total of L receive antennas are selected to convey the information bits, where there are a total of $\binom{K}{L}$ combinations of L receive antennas. For the RIS-RGSSK, the data bit stream is divided into $\lfloor \log_2 \binom{K}{L} \rfloor$ information bits, and then these bits are mapped to an index set $\mathcal{S}$ part of $\mathcal{C}$, where we denote $\mathcal{C}$ as the code-words set, i.e., the set of all combinations of receive-antenna indexes used at the transmitter. However, for the RIS-RGSM, the data bit stream is divided into $\lfloor \log_2 \binom{K}{L} \rfloor + L \log_2(M)$ information bits, where the most significant $\lfloor \log_2 \binom{K}{L} \rfloor$ bits are mapped to an index set $\mathcal{S}$ part of $\mathcal{C}$, and the least significant $L \log_2(M)$ bits are divided to form the PSK-modulated symbol per selected index. M is defined as the PSK modulation order to convey the additional information bits in the RIS-RGSM scheme. The RIS-RGSM with M-PSK allows non-coherent detection at the receiver, which significantly reduces the complexity and reduces the overhead of the receiver compared to amplitude-based ordinary modulations [7]. We represent the ordered set of selected receive-antenna indices as $\mathcal{S}$, with its lth element denoted by $\mathcal{S}(l)$ for $l = 1, \cdots, L$. For simplicity, we assume

an ascending order such that $\mathcal{S}(1) < \mathcal{S}(2) < \cdots < \mathcal{S}(L)$.

As described in [7], the optimization of the RIS-phases of the RIS-RGSSK and RIS-RGSM schemes utilizes the real part of the received signal. The real part of the signal received at the lth selected antenna is given by

$$y^{\mathcal{R}}_{\mathcal{S}(l)} = \sqrt{E_s}\left(\mathbf{h}^{\mathcal{R}}_{\mathcal{S}(l)}\boldsymbol{\theta}^{\mathcal{R}} - \mathbf{h}^{\mathcal{I}}_{\mathcal{S}(l)}\boldsymbol{\theta}^{\mathcal{I}}\right) + n^{\mathcal{R}}_{\mathcal{S}(l)}, \tag{4.2}$$

where $(\cdot)^{\mathcal{R}}$ and $(\cdot)^{\mathcal{I}}$ denote the real and imaginary parts of a complex scalar/vector, respectively. From (4.2), we can observe that $\boldsymbol{\theta}$ needs to be optimized to maximize the real part of the received signal at the kth received antennas. From [7], we consider the optimal solution for $\boldsymbol{\theta}$ to be:

$$\tilde{\theta}^{\mathcal{R}}_i = \frac{\lambda_1 h^{\mathcal{R}}_{\mathcal{S}(1),i} + \lambda_2 h^{\mathcal{R}}_{\mathcal{S}(2),i}}{\sqrt{\left(R_i(\lambda_1,\lambda_2)\right)^2 + \left(I_i(\lambda_1,\lambda_2)\right)^2}}, \tag{4.3}$$

for all $i = 1, 2, \ldots, N$, and

$$\tilde{\theta}^{\mathcal{I}}_i = \frac{-(\lambda_1 h^{\mathcal{I}}_{\mathcal{S}(1),i} + \lambda_2 h^{\mathcal{I}}_{\mathcal{S}(2),i})}{\sqrt{\left(R_i(\lambda_1,\lambda_2)\right)^2 + \left(I_i(\lambda_1,\lambda_2)\right)^2}}, \tag{4.4}$$

for all $i = 1, 2, \ldots, N$, where $R_i(\lambda_1, \lambda_2) = \lambda_1 h^{\mathcal{R}}_{\mathcal{S}(1),i} + \lambda_2 h^{\mathcal{R}}_{\mathcal{S}(2),i}$, and $I_i(\lambda_1, \lambda_2) = \lambda_1 h^{\mathcal{I}}_{\mathcal{S}(1),i} + \lambda_2 h^{\mathcal{I}}_{\mathcal{S}(2),i}$, and $\boldsymbol{\lambda} = \left[\lambda_1, \lambda_2\right]^T$ is a Lagrange multiplier vector used to find $\tilde{\boldsymbol{\theta}}$.

At the receiver, detectors I, II, and III are employed to detect the activated antenna indexes non-coherently. For the RIS-RGSSK scheme, detector I is used to detect $\mathcal{S}$, given by [7]

$$\hat{\mathcal{S}} = \arg\max\left\{y^{\mathcal{R}}_l\right\}. \tag{4.5}$$

For the RIS-RGSM scheme, two different detectors are used depending on the modulation scheme used for extra information bit transmission. Detector II is employed when BPSK is used, and detector III is used when M-PSK is utilized. They are expressed, respectively, as [7]

$$\hat{\mathcal{S}} = \arg\max\left|y^{\mathcal{R}}_l\right|, \tag{4.6}$$

$$\hat{\mathcal{S}} = \arg\max|y_l|. \tag{4.7}$$

where arg max {.} returns the maximum value of its argument.

In the subsequent sections, we delve into the performance analysis of the RIS-RGSSK and RIS-RGSM schemes, focusing on the PEP while utilizing detectors I, II, and III.

4.3 Performance Analysis

In this section, we derive the theoretical PEP of the RIS-RGSSK and RIS-RGSM systems. For which, we consider that $L = 2$ antennas are activated out of a receiver equipped with K receive antennas. Choosing $L = 2$ simplifies the analysis and makes the derivations tractable.

4.3.1 RIS-RGSSK scheme

In this section, we derive the theoretical PEP for the RIS-RGSSK scheme. This analysis is centered on detector I from [7]. Since $L = 2$, the set $\mathcal{S}$ groups two indexes $\mathcal{S}(1)$ and $\mathcal{S}(2)$. Our analysis focuses on the detection process related to antenna $\mathcal{S}(1)$. It is noteworthy that, due to the inherent symmetry between the detection of $\mathcal{S}(1)$ and $\mathcal{S}(2)$, the PEP expression for the detection of antenna $\mathcal{S}(2)$ is straightforward. Since detector I operates on the real part of the received signal, then, the PEP associated with the selected antenna $\mathcal{S}(1)$ and the detected antenna $\hat{\mathcal{S}}(1)$ can be expressed as:

$$\mathrm{PEP}_{\mathrm{RGSSK}}(\mathcal{S}(1), \hat{\mathcal{S}}(1)) = \Pr\left\{ \; y^{\mathcal{R}}_{\mathcal{S}(1)} < y^{\mathcal{R}}_{\hat{\mathcal{S}}(1)} \; \right\} \tag{4.8}$$

$$= \Pr\left\{ \left(\sqrt{E_s} \sum_{i=1}^{N} \left(h^{\mathcal{R}}_{\mathcal{S}(1),i} \theta^{\mathcal{R}}_i - h^{\mathcal{I}}_{\mathcal{S}(1),i} \theta^{\mathcal{I}}_i \right) + n^{\mathcal{R}}_{\mathcal{S}(1)} \right) \right.$$

$$\left. < \left(\sqrt{E_s} \sum_{i=1}^{N} \left(\; h^{\mathcal{R}}_{\hat{\mathcal{S}}(1),i} \theta^{\mathcal{R}}_i - h^{\mathcal{I}}_{\hat{\mathcal{S}}(1),i} \theta^{\mathcal{I}}_i \; \right) + n^{\mathcal{R}}_{\hat{\mathcal{S}}(1)} \right) \right\}. \tag{4.9}$$

By substituting (4.3) and (4.4) in (4.9) while considering that $\theta^{\mathcal{R}}_i$ and $\theta^{\mathcal{I}}_i$ take average values of λ_1 and λ_2 ($\lambda_1 = \lambda_2 = 1/2$) [6], the PEP can be upper bounded as

$$\mathrm{PEP}_{\mathrm{RGSSK}}(\mathcal{S}(1), \hat{\mathcal{S}}(1)) \leq \Pr\left(\left(\sqrt{E_s} Z + n^{\mathcal{R}}_{\mathcal{S}(1)} \right) < \left(\sqrt{E_s} \hat{Z} + n^{\mathcal{R}}_{\hat{\mathcal{S}}(1)} \right) \right), \tag{4.10}$$

where $Z = \sum_{i=1}^{N} Z_i = \sum_{i=1}^{N} \frac{A_i^2 + C_i^2 + A_i D_i + C_i B_i}{\sqrt{(A_i + D_i)^2 + (C_i + B_i)^2}}$ as shown in [6], and the channel coefficients $A_i = h^{\mathcal{R}}_{\mathcal{S}(1),i}$, $B_i = h^{\mathcal{I}}_{\mathcal{S}(2),i}$, $C_i = h^{\mathcal{I}}_{\mathcal{S}(1),i}$, and $D_i = h^{\mathcal{R}}_{\mathcal{S}(2),i}$, and $\hat{Z} = \sum_{i=1}^{N} \hat{Z}_i = \sum_{i=1}^{N} \left(\hat{A}_i \theta^{\mathcal{R}}_i - \hat{C}_i \theta^{\mathcal{I}}_i \right)$, where we define $\hat{A}_i = h^{\mathcal{R}}_{\hat{\mathcal{S}}(1),i}$, and $\hat{C}_i = h^{\mathcal{I}}_{\hat{\mathcal{S}}(1),i}$ to simplify the notation.

According to the central limit theorem, Z and $\hat{Z}$ both follow a normal distribution, i.e., $Z \sim \mathcal{N}\left(N\mathbb{E}\left\{Z_i\right\}, N\mathbb{V}\left\{Z_i\right\}\right)$ and $\hat{Z} \sim \mathcal{N}\left(N\mathbb{E}\left\{\hat{Z}_i\right\}, N\mathbb{V}\left\{\hat{Z}_i\right\}\right)$, where $\mathbb{E}\{.\}$ and $\mathbb{V}\{.\}$, respectively, denote the expectation and variance operator. Then, the expected value and variance of Z_i and $\hat{Z}_i$ can be derived by introducing the random variables (RVs) $X_A = \sqrt{E_s}Z + n^{\mathcal{R}}_{\mathcal{S}(1)}$ and $Y_A = \sqrt{E_s}\hat{Z} + n^{\mathcal{R}}_{\hat{\mathcal{S}}(1)}$, and referring to [6], the means and variances of RVs X_A and Y_A are: $\mathbb{E}\{X_A\} = \frac{N\sqrt{2\pi E_s}}{4}$, $\mathbb{V}\{X_A\} = N\left(\frac{6-\pi}{8}\right)E_s + \frac{N_0}{2}$, $\mathbb{E}\{Y_A\} = 0$, and $\mathbb{V}\{Y_A\} = \frac{NE_s}{2} + \frac{N_0}{2}$.

Thus, we can rewrite (4.10) as

$$\mathrm{PEP}_{\mathrm{RGSSK}}(\mathcal{S}(1), \hat{\mathcal{S}}(1)) \leqslant (F_A < 0), \tag{4.11}$$

where $F_A = X_A - Y_A$. Since F_A follows a normal distribution, its mean and variance can be calculated as $\mathbb{E}\{F_A\} = \mathbb{E}\{X_A\} - \mathbb{E}\{Y_A\} = \frac{N\sqrt{2\pi E_s}}{4}$, and $\mathbb{V}\{F_A\} = \mathbb{V}\{X_A\} + \mathbb{V}\{Y_A\} = \frac{NE_s(10-\pi)}{8} + N_0$. In [6], all the antenna indexes are detected using the squared real or imaginary parts of the received signal, which forces the PEP analysis to involve chi-square or related distributions. Unlike [6], here, because of detector I, F_A has a normal distribution, and hence, the probability density function of F_A can be expressed as

$$f(F_A) = \frac{1}{\sqrt{2\pi\mathbb{V}\{F_A\}}} \exp\left(-\frac{(F_A - \mathbb{E}\{F_A\})^2}{2\mathbb{V}\{F_A\}}\right). \tag{4.12}$$

Then, with simple manipulations, the PEP, which represents the cumulative distribution function (CDF) of F_A, can be written using the error function (erf) as

$$\mathrm{PEP}_{\mathrm{RGSSK}}(\mathcal{S}(1), \hat{\mathcal{S}}(1)) \leq \frac{1}{2}\left(1 + \mathrm{erf}\left(\frac{-N\sqrt{2\pi E_s}}{2\sqrt{8N_0 - NE_s(\pi - 10)}}\right)\right), \tag{4.13}$$

where $\mathrm{erf}(F_A)$ is defined as $\frac{2}{\sqrt{\pi}}\int_0^{F_A} e^{-t^2}\,dt$. This PEP is obtained by simply evaluating (4.13), contrary to [6] where due to its detector, numerical methods and approximations are necessary to obtain upper bounds on the PEP results.

4.3.2 RIS-RGSM scheme with BPSK

In this section, we derive the PEP for the RIS-RGSM scheme with BPSK. This derivation is based on detector II [7]. The PEP associated with the selected antenna $\mathcal{S}(1)$ and the

detected antenna $\hat{\mathcal{S}}(1)$ can be expressed as:

$$\mathrm{PEP}_{\mathrm{RGSM}}(\mathcal{S}(1),\hat{\mathcal{S}}(1)) = \Pr\left\{\left|y^{\mathcal{R}}_{\mathcal{S}(1)}\right|^2 < \left|y^{\mathcal{R}}_{\hat{\mathcal{S}}(1)}\right|^2\right\}. \tag{4.14}$$

Here, $y^{\mathcal{R}}_{\mathcal{S}(1)}$ and $y^{\mathcal{R}}_{\hat{\mathcal{S}}(1)}$ are approximated as Gaussian RVs. Then, we can rewrite the PEP as

$$\mathrm{PEP}_{\mathrm{RGSM}}(\mathcal{S}(1),\hat{\mathcal{S}}(1)) \leq \Pr\left(F_B \leq 1\right), \tag{4.15}$$

where F_B is equals to X_A^2/Y_A^2. Here, X_A^2 is a non-central ($\mathbb{E}\{X_A\} \neq 0$) chi-square (χ^2_{d1}) RV with one degree of freedom ($d_1 = 1$), and Y_A^2 is a central ($\mathbb{E}\{Y_A\} = 0$) chi-square (χ^2_{d2}) RV with one degree of freedom ($d_2 = 1$). The PEP in [6] also involves two chi-square RVs; however, the procedure in [6] is based on the subtraction of these two RVs and does not end in a closed-form expression, but in numerical methods and approximations. Unlike that, (4.15) as a ratio allows us to derive a compact form expression for the PEP.

To obtain the PEP, we use the Fisher–Snedecor (F)-distribution [8]. The F-distribution with d_1 and d_2 degrees of freedom is defined as the distribution of

$$F_{d_1,d_2} \equiv \frac{\chi^2_{d_1}/d_1}{\chi^2_{d_2}/d_2}, \tag{4.16}$$

where $\chi^2_{d_1}$ and $\chi^2_{d_2}$ are independent RV with chi-square distributions with respective degrees of freedom d_1 and d_2.

Then, we have that the CDF of the F-distribution in (4.16) is defined as [9]

$$F\left(x, d_1, d_2, \delta\right) = \sum_{j=0}^{\infty}\left(\frac{\left(\frac{1}{2}\delta\right)^j}{j!}e^{\frac{-\delta}{2}}\right) I\left(\frac{d_1\cdot x}{d_2 + d_1\cdot x}\middle|\ \frac{d_1}{2}+j, \frac{d_2}{2}\right), \tag{4.17}$$

where $I(x|a_0, b_0)$ is the incomplete beta function with parameters a_0 and b_0 evaluated in x, and δ is the positive non-centrality parameter. However, our objective in (4.15) is to determine the probability that $\Pr(X_A^2/Y_A^2 \leq 1)$, hence, we aim to rewrite the F-distribution to conveniently apply (4.17). We can then take the normally distributed RVs X_A and Y_A and square them to obtain the RVs $X_A^2 = \sigma^2_{X_A}\chi^2_{d_1}$ and $Y_A^2 = \sigma^2_{Y_A}\chi^2_{d_2}$, where $\sigma^2_{X_A}$ and $\sigma^2_{Y_A}$ are the variances of X_A and Y_A, respectively. Now, by substituting $\chi^2_{d_1}$ and $\chi^2_{d_2}$ in (4.16), we rewrite the F-ratio as

$$F_{d_1,d_2} \equiv \frac{\sigma^2_{Y_A}X_A^2/d_1}{\sigma^2_{X_A}Y_A^2/d_2}. \tag{4.18}$$

The ratio in (4.18) is a scaled version of (4.16) by $\frac{\sigma^2_{Y_A}}{\sigma^2_{X_A}}$, we can, then, obtain the PEP by evaluating the CDF of (4.18) as a scaled version of the CDF in (4.17), for which $x = \frac{\sigma^2_{Y_A}}{\sigma^2_{X_A}}$. Here, the positive non-centrality parameter δ is defined as $\mu^2_{X_A}/\sigma^2_{X_A}$ [8]. Then, the PEP is expressed as

$$\mathrm{PEP}_{\mathrm{RGSM}}(\mathcal{S}(1), \hat{\mathcal{S}}(1)) = F\left(\frac{\sigma^2_{Y_A}}{\sigma^2_{X_A}}, d_1, d_2, \frac{\mu^2_{X_A}}{\sigma^2_{X_A}}\right). \tag{4.19}$$

Now, we simply substitute the mean and variance of X_A and Y_A in (4.19) to obtain the PEP. Here, $\mu_{X_A} = \frac{N\sqrt{2\pi E_s}}{4}$, $\sigma^2_{X_A} = N\left(\frac{6-\pi}{8}\right)E_s + \frac{N_0}{2}$, $\mu_{Y_A} = 0$, and $\sigma^2_{Y_A} = \frac{NE_s+N_0}{2}$, which are the same parameters used in Section 4.3.1.

4.3.3 RIS-RGSM Scheme with M-PSK

In this section, we derive the PEP for the RIS-RGSM system using M-PSK. Here, we focus on detector III [7]. The PEP corresponding to the selected antenna $\mathcal{S}(1)$ and the detected antenna $\hat{\mathcal{S}}(1)$ can be expressed as:

$$\mathrm{PEP}_{\mathrm{RGSM}}(\mathcal{S}(1), \hat{\mathcal{S}}(1)) = \Pr\left\{|X_C|^2 - |Y_C|^2 < 0\right\}, \tag{4.20}$$

where, $X_C = y_{\mathcal{S}(1)}$, and $Y_C = y_{\hat{\mathcal{S}}(1)}$. Different from the PEPs in Sections 4.3.1 and 4.3.2, the PEP in (4.20) considers both real and imaginary components of the RVs X_C and Y_C as described by detector III. In [6], the implemented detector for the PEP derivation only uses the squared real or imaginary part of the received signal, which means that one of the two components of the received signal does not impact the associated RVs to obtain the PEPs, and hence, the PEPs in [6] differs from (4.20). To evaluate (4.20), we follow the probability as a general case of the quadratic function of the form $\Pr\left(|X_C|^2 - |Y_C|^2 < 0\right)$ defined in [10], which is equivalent to our case in (4.20). Here, the pairs $\{X_C, Y_C\}$ are mutually statistically independent and identically distributed. Then, the PEP is stated as [10]

$$\mathrm{PEP}_{\mathrm{RGSM}}(\mathcal{S}(1), \hat{\mathcal{S}}(1)) = Q_1(r,s) - \frac{b_2/b_1}{1+b_2/b_1} I_0(rs) \exp\left[-\frac{1}{2}\left(r^2+s^2\right)\right], \tag{4.21}$$

where the Marcum Q function is defined as [10]

$$Q_1(r,s) = \exp\left[-\frac{1}{2}\left(r^2+s^2\right)\right] + \sum_{i=0}^{\infty}\left(\frac{r}{s}\right)^i I_i(rs), \tag{4.22}$$

and $I_i(rs)$ denotes the ith-order modified Bessel function defined as [10]

$$I_i(rs) = \begin{cases} \frac{1}{2\pi j}\left(\frac{r}{s}\right)^i \int_\Gamma \frac{1}{p^{i+1}} \exp\left(\frac{\frac{1}{2}r^2}{p} + \frac{1}{2}s^2 p\right) \mathrm{d}p, \\ \frac{1}{2\pi j}\left(\frac{s}{r}\right)^i \int_\Gamma p^{i-1} \exp\left(\frac{\frac{1}{2}r^2}{p} + \frac{1}{2}s^2 p\right) \mathrm{d}p. \end{cases} \tag{4.23}$$

As well as the coefficients r, s, b_1, b_2, α_1, α_2, $\mu_{x_C y_C}$, $\mu_{x_C x_C}$, $\mu_{y_C y_C}$ and u are defined as follows [10]

$$r = \left[\frac{2b_1^2 b_2\left(\alpha_1 b_2 - \alpha_2\right)}{\left(b_1+b_2\right)^2}\right]^{1/2}, \tag{4.24}$$

$$s = \left[\frac{2b_1 b_2^2\left(\alpha_1 v_1 + \alpha_2\right)}{\left(b_1+b_2\right)^2}\right]^{1/2}, \tag{4.25}$$

$$b_1 = \sqrt{u^2 + \frac{1}{4\left(\mu_{x_C x_C}\mu_{y_C y_C} - \left|\mu_{x_C y_C}\right|^2\right)}} - u, \tag{4.26}$$

$$b_2 = \sqrt{u^2 + \frac{1}{4\left(\mu_{x_C x_C}\mu_{y_C y_C} - \left|\mu_{x_C y_C}\right|^2\right)}} + u, \tag{4.27}$$

$$u = \frac{\mu_{x_C x_C} - \mu_{y_C y_C}}{4\left(\mu_{x_C x_C}\mu_{y_C y_C} - \left|\mu_{x_C y_C}\right|^2\right)}, \tag{4.28}$$

$$\alpha_1 = 2\left(\left|\mu_{X_C}\right|^2 \mu_{y_C y_C} + \left|\mu_{Y_C}\right|^2 \mu_{x_C x_C}\right), \tag{4.29}$$

$$\alpha_2 = \left|\mu_{X_C}\right|^2 - \left|\mu_{Y_C}\right|^2, \tag{4.30}$$

$$\mu_{x_C y_C} = \frac{1}{2}\mathbb{E}\left[\left(X_C - \mu_{X_C}\right)\left(Y_C - \mu_{Y_C}\right)^*\right], \tag{4.31}$$

$$\mu_{x_C x_C} = \frac{1}{2}\sigma_{X_C}^2, \tag{4.32}$$

$$\mu_{y_C y_C} = \frac{1}{2}\sigma_{Y_C}^2. \tag{4.33}$$

Here, $\mu_{xy} = 0$ due to the independence of X_C and Y_C. To evaluate (4.21), we require the mean and variance of X_C and Y_C. Referring to [6], we find the expected value of X_C (μ_{X_C}) to be $\frac{N\sqrt{2\pi E_s}}{4}$, and its variance $\sigma_{X_C}^2 = N\left(\frac{8-\pi}{8}\right)E_s + N_0$. For Y_C, its mean is $\mu_{Y_C} = 0$ and its variance is $\sigma_{Y_C}^2 = NE_s + N_0$.

To simplify (4.21) into a closed-form expression, we first reduce u in (4.28) to

$$u = \frac{1}{4\mu_{y_C y_C}} - \frac{1}{4\mu_{x_C x_C}}. \tag{4.34}$$

Then, by substituting (4.34) into (4.26) and (4.27), we obtain

$$b_1 = \frac{1}{2} \cdot \frac{1}{\mu_{x_C x_C}}, \tag{4.35}$$

$$b_2 = \frac{1}{2} \cdot \frac{1}{\mu_{y_C y_C}}. \tag{4.36}$$

By substituting (4.32) and (4.33) in (4.35) and (4.36), respectively, we obtain

$$b_1 = \frac{1}{\sigma^2_{X_C}} = \frac{1}{N\left(\frac{8-\pi}{8}\right)E_s + N_0}, \tag{4.37}$$

$$b_2 = \frac{1}{\sigma^2_{Y_C}} = \frac{1}{NE_s + N_0}. \tag{4.38}$$

Further manipulations reveal that r in (4.24) equals zero, and s in (4.25) is reduced to

$$s = \frac{|\mu_{X_C}|^2}{\mu_{x_C x_C} + \mu_{y_C y_C}}. \tag{4.39}$$

Then, by substituting (4.32) and (4.33) in (4.39), we obtain

$$s = \frac{2|\mu_{X_C}|^2}{\sigma^2_{X_C} + \sigma^2_{Y_C}} = \frac{N^2 E_s \pi}{8N_0 + NE_s\frac{16-\pi}{2}}. \tag{4.40}$$

Utilizing (4.22), we can find $Q_1(r, s)$ for $r = 0$ as

$$Q_1(0, s) = \exp\left(-\frac{1}{2}s^2\right). \tag{4.41}$$

By substituting (4.41) and $I_0(0) = 1$ from (4.23) in (4.21), we obtain the PEP as:

$$\mathrm{PEP}_{\mathrm{RGSM}}(\mathcal{S}(1), \hat{\mathcal{S}}(1)) = (1 - \frac{b_2}{b_1 + b_2}) \exp(-\frac{1}{2}s^2). \tag{4.42}$$

Then, after substituting (4.37), (4.38), and (4.40) in (4.42) the PEP is expressed as

$$\mathrm{PEP}_{\mathrm{RGSM}}(\mathcal{S}(1), \hat{\mathcal{S}}(1)) = \frac{1 + N\frac{E_s}{N_0}}{2 + \left(2 - \frac{\pi}{8}\right)N\frac{E_s}{N_0}} \times \exp\left(-\frac{\pi N^2 \frac{E_s}{N_0}}{16 + (16-\pi)N\frac{E_s}{N_0}}\right). \tag{4.43}$$

4.4 Simulation Results

Fig. 4.2 compares the results of the theoretical PEP (using approximated $\boldsymbol{\lambda}$) with the simulated PEP for the RIS-RGSSK (also utilizing an approximated $\boldsymbol{\lambda}$ for fairness). Here, $L = 2$, and $N = 64, 128$, and 256. It is observed that the analytical results align with the simulation-based PEP results.

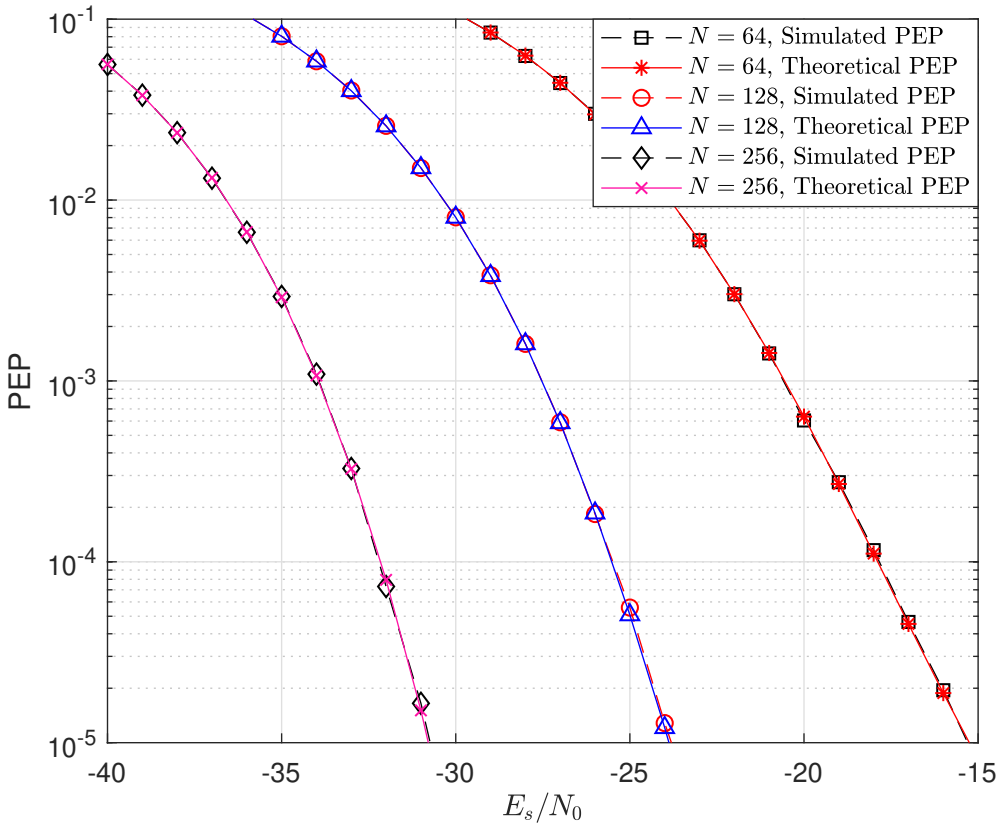

Figure 4.2: Theoretical PEP and simulated-based PEP results of the proposed RIS-RGSSK scheme at $N = 64$, 128, and 256 for $L = 2$.

Fig. 4.3 illustrates the PEPs of the RIS-RGSM with BPSK, showcasing both theoretical and simulation-based results employing approximated $\boldsymbol{\lambda}$. The figure contrasts the theoretical outcomes based on the F-distribution with the simulated PEPs for $N = 64$, 128, and 256. Notably, the simulation results closely align with the theoretical PEPs across all observed values of N and E_s/N_0.

In Fig. 4.4, the PEPs of the RIS-RGSM with M-PSK are depicted, presenting both theoretical and simulation-based results using approximated $\boldsymbol{\lambda}$. The theoretical PEP, derived from a closed-form expression based on the probability of a special case of the general quadratic form in [10], offers valuable insights into the system's performance for $N = 64$, 128, and 256. Overall, a notable alignment between simulation and analytical results is observed. However, some discrepancies are noticeable, particularly showing a difference of

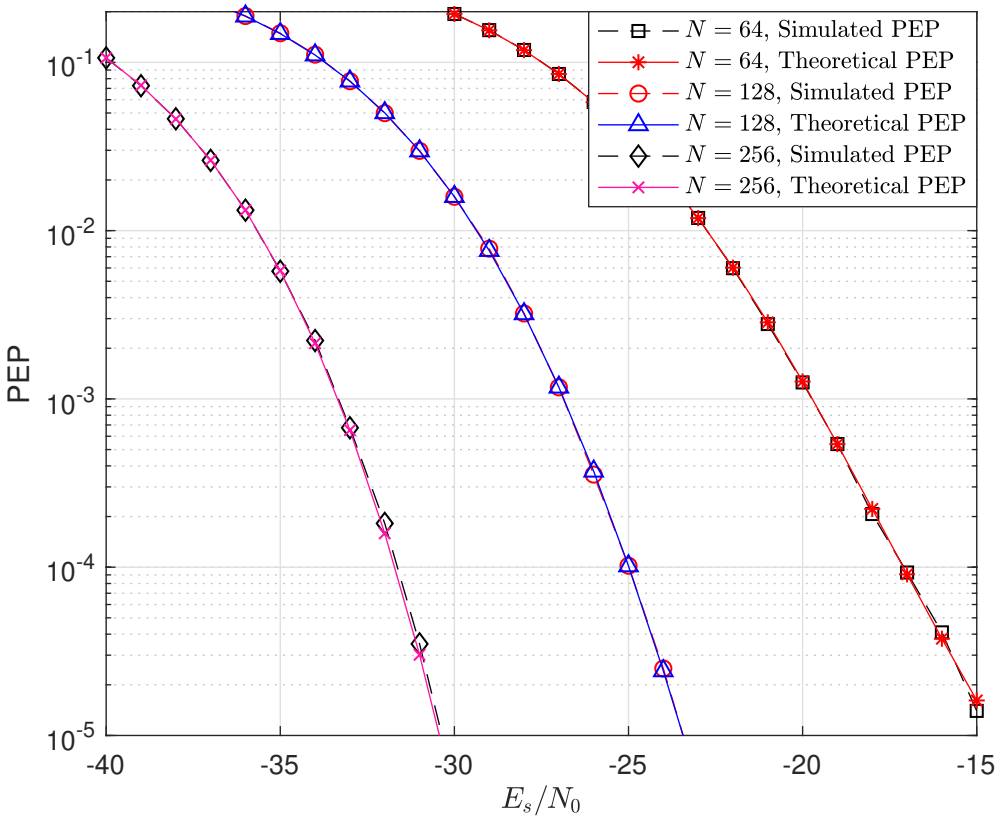

Figure 4.3: Theoretical PEP and simulated-based PEP results of the proposed RIS-RGSM scheme with BPSK at $N = 64$, 128, and 256 for $L = 2$.

about 0.5 dB in PEPs for smaller N ($N = 64$), which can be attributed to the unequal statistics between X_C and Y_C. As N increases, this difference becomes insignificant.

4.5 Conclusion

In this paper, we conducted a performance analysis, specifically focusing on the PEP, for two schemes: RIS-RGSSK and RIS-RGSM. We investigated and provided the detailed performance for the RIS-RGSSK scheme, which exhibited a normal distribution, enabling a clear and thorough analysis of its performance without requiring numerical methods and/or approximations. For RIS-RGSM, we derived the PEP for both BPSK and M-PSK cases. Utilizing an F-distribution, we derived the closed-form expression for the PEP of RIS-RGSM with BPSK, and derived the PEP for the RIS-RGSM with M-PSK by applying a special

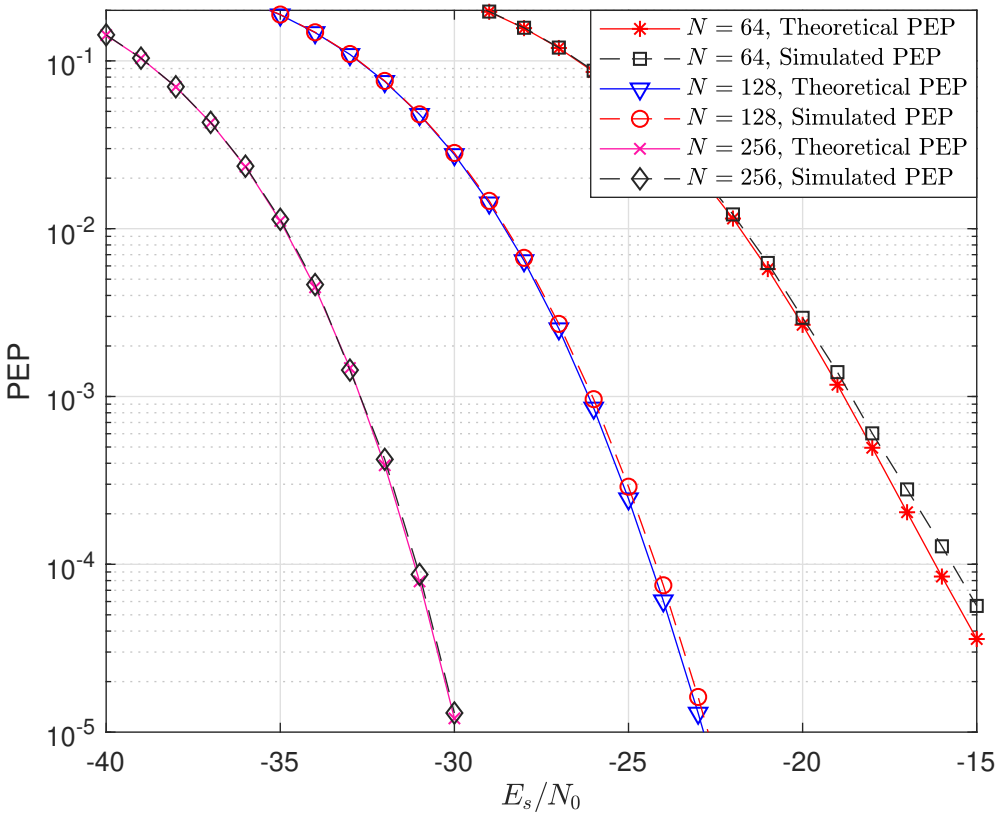

Figure 4.4: Theoretical PEP and simulated-based PEP results of the proposed RIS-RGSM scheme with M-PSK at $N = 64$, 128, and 256 for $L = 2$.

case of the quadratic form of probabilities. We verified our analytical findings with simulated results.

References

[1] E. Basar, M. Di Renzo, J. De Rosny, M. Debbah, M.-S. Alouini, and R. Zhang, "Wireless communications through reconfigurable intelligent surfaces," *IEEE Access*, vol. 7, pp. 116 753–116 773, 2019.

[2] X. Zhu, W. Chen, Q. Wu, Z. Li, J. Li, S. Zhang, and M. Ding, "Reconfigurable intelligent surface aided space shift keying with imperfect CSI," *IEEE Internet Things J.*, Nov. 2023.

[3] A. E. Canbilen, E. Basar, and S. S. Ikki, "Reconfigurable intelligent surface-assisted space shift keying," *IEEE Wireless Commun. Lett.*, vol. 9, no. 9, pp. 1495–1499, Jan. 2020.

[4] S. Lin, B. Zheng, G. C. Alexandropoulos, M. Wen, M. Di Renzo, and F. Chen, "Reconfigurable intelligent surfaces with reflection pattern modulation: Beamforming design and performance analysis," *IEEE Trans. Wireless Commun.*, vol. 20, no. 2, pp. 741–754, Feb. 2021.

[5] E. Basar, "Reconfigurable intelligent surface-based index modulation: A new beyond MIMO paradigm for 6G," *IEEE Trans. Commun.*, vol. 68, no. 5, pp. 3187–3196, May 2020.

[6] M. H. Dinan, N. S. Perović, and M. F. Flanagan, "RIS-assisted receive quadrature space-shift keying: A new paradigm and performance analysis," *IEEE Trans. Commun.*, vol. 70, no. 3, pp. 6874–6889, Oct. 2022.

[7] P. A. Marín, M. Hanif, and E. Bedeer, "RIS-assisted receive generalized space shift keying and receive generalized spatial modulation," *IEEE Wirel. Commun. Lett.*, vol. 13, no. 10, pp. 2712–2716, Aug. 2024.

[8] R. E. Kirk, *Experimental Design: Procedures for the Behavioral Sciences*, 4th ed. Thousand Oaks, CA: Sage, 2013.

[9] N. Johnson and S. Kotz, *Distributions in Statistics: Continuous Univariate Distributions-2*. Hoboken, NJ: John Wiley & Sons, Inc., 1970.

[10] J. G. Proakis and M. Salehi, *Digital communications*. McGraw-hill, 2008.

5. Conclusions and Suggested Future Studies

5.1 Conclusions

We have presented two modulation schemes that combine RIS-assisted systems with IM in this work. The main objective of these schemes is to improve the SE of future wireless communication systems. The main contributions of our work are given as follows:

In Chapter 3, we presented two schemes RIS-RGSSK and RIS-RGSM that we proposed to enhance system performance in terms of the SE. We formulated and solved an optimization problem to maximize the minimum value of the real part of the received signals at all the selected receive antennas. First, we solved this optimization problem for the RIS-RGSSK scheme, and then we extended the optimization solution to the RIS-RGSM scheme. Additionally, we presented non-coherent GDs for both schemes. We also analyzed the complexity of the proposed GDs and compared them with the optimal ML detector, and demonstrated that the GDs, while maintaining efficient performance, had lower complexity than the optimal ML detector. The simulation results showed that the proposed RIS-RGSM scheme outperforms existing schemes like RIS-RQSSK by achieving better BER performance and higher bit rates. Particularly noteworthy is the 4.0 dB improvement in E_b/N_0 when $N = 256$ for the RIS-RGSM scheme compared to the benchmark scheme.

In Chapter 4, we thoroughly analyzed the performance of the proposed RIS-RGSSK and RIS-RGSM schemes, with a particular focus on finding their PEP. For the RIS-RGSSK scheme, the RVs used to compute the PEP followed a normal distribution, offering a straightforward evaluation of the PEP. In contrast, for the RIS-RGSM scheme, we derived the PEP for both cases: using BPSK and M-PSK modulation schemes. Specifically, we obtained a

closed-form expression for the PEP of RIS-RGSM with BPSK using an F-distribution and employed generalized quadratic form probability to derive the PEP for the M-PSK case. The simulation results verified our performance analysis of both schemes.

5.2 Future Research Topics

Several future research directions for RIS-assisted IM that can be explored include:

- For both of our schemes, RIS-RGSSK and RIS-RGSM, as well as many other schemes in the literature, we assumed complete knowledge of the channel between the RIS elements and the receive antennas. This highlights the need for channel modeling and estimation in future research.

- Another point is that both the RIS-RGSSK and RIS-RGSM schemes, as well as many other schemes in the literature, are assumed to operate in static environments, meaning they do not account for mobility. Future research directions for RIS in wireless communication systems should consider mobility within network environments, allowing applications such as vehicles and UAVs. Mobility introduces changing channel conditions, which shows the need for advanced channel estimation techniques capable of accurately tracking these changes. This scenario will also require new optimal RIS shift optimizations. Additionally, integrating mobility into RIS-based systems will demand efficient signal processing strategies to handle the increased complexity associated with frequent updates to channel estimations.